Retinal metabolism: Evidence for uncoupling of glycolysis and oxidative phosphorylation via Cori-, Cahill-, and mini-Krebs-cycle

Yiyi Chen[1, 5], Laimdota Zizmare[2, 5], Victor Calbiague[3], Lan Wang[1], Shirley Yu[1], Friedrich W. Herberg[4], Oliver Schmachtenberg[3], François Paquet-Durand[1, 5, 6*], Christoph Trautwein[2, 5*]

[1] Institute for Ophthalmic Research, University of Tübingen, 72076, Germany

[2] Werner Siemens Imaging Center, Department of Preclinical Imaging and Radiopharmacy, University of Tübingen, 72076, Germany

[3] Centro Interdisciplinario de Neurociencia de Valparaíso, Universidad de Valparaíso, Chile

[4] Biochemistry Department, University of Kassel, 34132, Germany

[5] These authors contributed equally

[6] Lead contact

* Corresponding authors: François Paquet-Durand, Christoph Trautwein.

Email: francois.paquet-durand@klinikum.uni-tuebingen.de
christoph.trautwein@med.uni-tuebingen.de

Highlights

- The retina utilizes a complex energy switchboard consisting of the Krebs cycle, mini-Krebs cycle, Cahill cycle, and Cori cycle.
- Mini-Krebs cycle runs more efficiently than 'full' Krebs cycle.
- Alanine transaminase decouples glycolysis from the Krebs cycle.
- Lactate, alanine, and N-acetylaspartate are distinctive energetic pathway signatures.

Abstract

The retina consumes massive amounts of energy, yet its metabolism and substrate exploitation remain poorly understood. Here, we used a murine explant model to manipulate retinal energy metabolism under entirely controlled conditions and utilized ^{1}H-NMR spectroscopy-based metabolomics, *in situ* enzyme detection, and cell viability readouts to uncover the pathways of retinal energy production. Our experimental manipulations resulted in varying degrees of photoreceptor degeneration, while the inner retina and retinal pigment epithelium were essentially unaffected. This selective vulnerability of photoreceptors suggested very specific adaptations in their energy metabolism. Rod photoreceptors were found to rely strongly on oxidative phosphorylation, but only mildly on glycolysis. Conversely, cone photoreceptors were dependent on glycolysis but insensitive to electron transport chain decoupling. Importantly, photoreceptors appeared to uncouple glycolytic and Krebs-cycle metabolism via three different pathways: 1) the mini-Krebs-cycle, fueled by glutamine and branched-chain amino acids, generating N-acetylaspartate; 2) the alanine-generating Cahill-cycle; 3) the lactate-releasing Cori-cycle. Moreover, the metabolomic data indicated a shuttling of taurine and hypotaurine between the retinal pigment epithelium and photoreceptors, likely resulting in an additional net transfer of reducing power to photoreceptors. These findings expand our understanding of retinal physiology and pathology and shed new light on neuronal energy homeostasis and the pathogenesis of neurodegenerative diseases.

Keywords

Energy homeostasis, glucose transport, aerobic glycolysis, glucose-alanine cycle, alanine transaminase, aspartate amino transferase

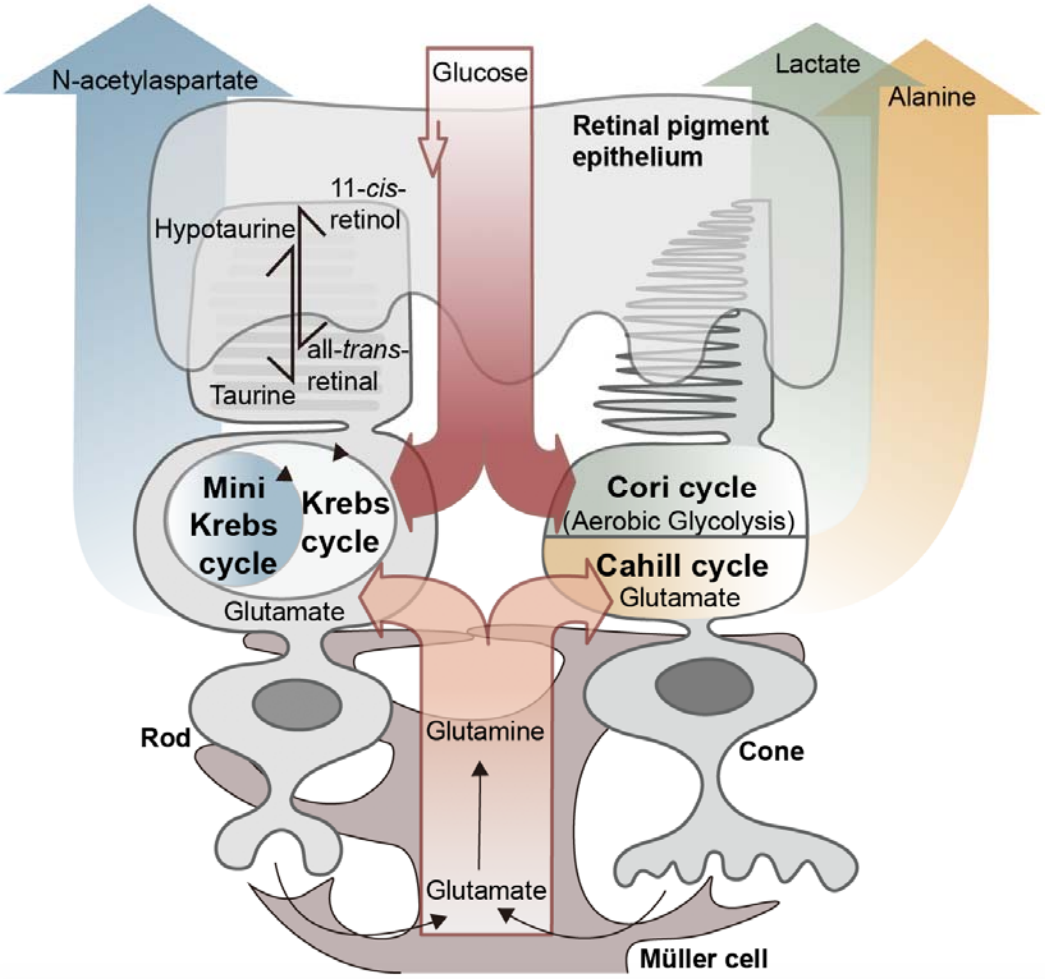

Graphical abstract: Retinal photoreceptors employ both glucose and glutamate as fuels. While rod photoreceptors rely strongly on oxidative phosphorylation and the N-acetylaspartate producing mini-Krebs-cycle, cone photoreceptors rely on the lactate-producing Cori cycle and the oxidative, alanine-producing Cahill cycle.

Abbreviations

1,9-DDF – 1,9 dideoxyforskolin, AA – amino acids, AST – aspartate amino transferase, ADP – adenosine diphosphate, ALT – alanine transaminase, ATP – adenosine triphosphate, BCAA – branched chain amino acid, COX – cytochrome oxidase, GAC – glutaminase C, GCs – ganglion cells, GLUT - glucose transporter, GS – glutamine synthase, GTP – guanosine triphosphate, GABA – gamma amino butyric acid, GPC – sn-glycero-3-phosphate, FCCP – carbonyl cyanide-*p*-trifluoromethoxyphenylhydrazone, GSSG – glutathione disulfide, INL – inner nuclear layer, MGC – Müller glial cells, NAA – N-acetylaspartate, NAD^+ – nicotinamide adenine dinucleotide, ONL – outer nuclear layer, O-PE – O-phosphoethanolamine, OXPHOS – oxidative phosphorylation, PARP – poly(ADP)ribose polymerase, PCK – phosphoenolpyruvate carboxy kinase, PKM – pyruvate kinase M, PNA - peanut agglutinin, RP – retinitis pigmentosa, RPE – retinal pigment epithelium, RPE65 – retinal pigment epithelium-specific 65 kDa protein, SUCLG1 – succinate-CoA ligase-1, TUNEL – terminal UDP nick-end labelling, UDP – uracil diphosphate

Introduction

The retina is the neuronal tissue with the highest energy demand (1, 2). Paradoxically, the mammalian retina is thought to strongly rely on energy-inefficient glycolysis, even though oxygen is available and high-yield oxidative phosphorylation (OXPHOS) possible (3). This aerobic glycolysis releases large amounts of lactate, as already reported in the 1920s by Otto Warburg (4). High retinal energy demand is linked to the extraordinary single-photon sensitivity of photoreceptors (2, 5, 6), and to lipid synthesis for the constant renewal of photoreceptor outer segments (7, 8).

The retina harbors two types of photoreceptors: rods, which exhibit remarkable light sensitivity and enable night vision; and cones, which work in daylight and allow color vision. Cones spend around twice as much energy as rods (9). Photoreceptors are not connected to the vasculature and are nourished by other retinal cell types, including retinal pigment epithelial (RPE) (10) cells or Müller glial cells (MGC). Moreover, photoreceptors can experience changes in energy demand on a millisecond timescale, from very high in the dark, to 4-10 times lower in light (5).

Glycolysis provides for rapid but inefficient adenosine triphosphate (ATP) production, while Krebs-cycle and OXPHOS are very efficient but much slower. Since glycolysis and Krebs-cycle are metabolically coupled through pyruvate, it is unclear how photoreceptors adapt to sudden and large changes in energy demand, and what energy substrates they may use. A recent hypothesis proposed that photoreceptors use predominantly aerobic glycolysis, with the resultant lactate utilized by the RPE and MGCs for OXPHOS (11). Such an arrangement would be reminiscent of the Cori-cycle, in which glucose and lactate are cycled between skeletal muscle and liver (12). However, this concept contrasts with the high density of mitochondria in photoreceptor inner segments, which strongly suggest an extensive use of OXPHOS.

Alternative pathways for ATP-generation include the Cahill-cycle, where pyruvate is transaminated using, for instance, glutamate to yield alanine and α-ketoglutarate (13, 14). The advantage of Cahill- over Cori-cycle is that reducing equivalents (*i.e.* NADH) gained during glycolysis are preserved and that α-ketoglutarate can yield additional ATP in mitochondrial OXPHOS. A second alternative may be the so-called mini-Krebs-cycle, in which a transamination of oxaloacetate with glutamate produces aspartate and α-ketoglutarate (15). This shortens the "full" 10-step Krebs-cycle to a significantly faster 6-step cycle. A point that Cori-, Cahill-, and mini-Krebs-cycle have in common is that they do not require the pyruvate-coupling between cytoplasmic glycolysis and mitochondrial OXPHOS, allowing both processes to run independent of each other. Whatever the case in the retina, the question as to which pathway is used has obvious ramifications for disease pathogenesis, including for diabetic retinopathy, age-related macular degeneration, or inherited retinal diseases, such as retinitis pigmentosa.

Here, we studied the expression of energy metabolism-related enzymes in different retinal cell types, using organotypic retinal explants maintained in serum-free, fully defined medium. Metabolic functions of the RPE were investigated by culturing retina with and without RPE. As readouts, we correlated enzyme expression with quantitative proton nuclear magnetic resonance (^{1}H-NMR) spectroscopy-based metabolomics and cell death. Notably, interventions in energy metabolism caused selective photoreceptor cell death, while leaving other retinal cell types essentially unaffected. Metabolomic analysis and localization of key enzymes identified important pathways and shuttles altered, explaining the strong interdependence of the various retinal cell types, and opening new perspectives for the treatment of neurodegenerative diseases in the retina and beyond.

Results

Retinal expression patterns of key energy metabolism related enzymes

We used immunofluorescence to assess expression and cellular localization of enzymes important for energy metabolism in wild-type mouse retina *in vivo* (Figure 1). The outermost retinal layer is formed by

RPE cells expressing RPE-specific 65kDa protein (RPE65), dedicated to the recycling of photopigment, retinal (16). Hence, RPE65 immunolabeling revealed the RPE cell monolayer (Figure 1A). Immunofluorescence for glucose-transporter-1 (GLUT1) showed strong labelling on basal and apical sides of RPE cells (Figure 1A), in line with previous literature (3, 17). GLUT1 expression was not detected in rods or cones (Supplementary Figure 1A, B). Instead, glucose uptake in the outer retina seems to be mediated by high affinity/high capacity GLUT3 (18), strongly expressed on photoreceptor inner segments (Supplementary Figure 2A). Pyruvate kinase is essential to glycolysis, catalyzing the conversion of phosphoenolpyruvate to pyruvate. While pyruvate kinase M1 (PKM1) was expressed in the inner retina (Supplementary Figure 2A), PKM2 was found in photoreceptor inner segments and synapses (Figure 1A). Expression of mitochondrial cytochrome oxidase (COX) largely overlapped with PKM2 (Figure 1A).

Challenging energy metabolism reduces rod and cone photoreceptor viability

To dissect retinal energy metabolism, we selectively manipulated key pathways (Figure 1B) using organotypic retinal explants (19) (Supplementary Figure 2B). Retinal cultures were prepared with the RPE cell layer attached to the neuroretina (control) or without RPE (*no* RPE). The *in vivo* expression patterns of enzymes important for energy metabolism (Figure 1A) were comparable in the *in vitro* situation (Supplementary Figure 2C). In control, the rate of cell death in the outer nuclear layer (ONL), as assessed by the TUNEL assay (Figure 1C, D), was low (0.46%±0.22, n=9). The *no* RPE condition displayed significantly increased photoreceptor cell death (3.35%±1.62, n=5, $p<0.001$). Blocking RPE glucose transport with the selective GLUT1 inhibitor 1,9-dideoxyforskolin (1,9-DDF) (18) further increased ONL cell death (6.77%±1.57, n=5, $p<0.0001$). The inhibition of glycolytic PKM2 with Shikonin (20), and OXPHOS disruption with the electron chain uncoupler carbonyl cyanide-p-trifluoromethoxyphenylhydrazone (FCCP) (16) both caused a significant increase in photoreceptor cell death (Shikonin: 17.75%±2.13, n=5, $p<0.0001$; FCCP: 22.49 % ± 6.79, n=5, $p<0.0001$). All four experimental interventions mostly affected photoreceptors, not significantly reducing the viability of other retinal cell types (Figure 1C).

Remarkably, a differential effect on cone photoreceptor survival (Figure 1E, F) was observed as assessed by immunodetection of the cone-specific marker arrestin-3 (Arr3). Control retina harbored 11.47 (±1.95, n=9) cones per 100 µm of retinal circumference. *no* RPE retina displayed a significant decrease in cone survival (4.62±1.39, n=5, $p<0.0001$), while blocking RPE glucose transport with 1,9-DDF led to an even more dramatic reduction (1.02±1.09, n=5, $p<0.0001$). By comparison, inhibition of glycolysis with Shikonin had a relatively mild effect on cone survival (7.78±1.36, n=5, $p<0.0001$). Surprisingly, FCCP treatment did not cause cone death (12.84±1.75, n=5, $p=0.22$), compared to control.

We further calculated the percentages of dying cones and rods, assuming that 3% of all photoreceptors were cones (21, 22) (Figure 1G, H). In the four treatment situations the ratios of cone to rod death were: *no* RPE = 1:1; 1,9-DDF = 1:1.5; Shikonin = 1:17; and FCCP = 0: ∞. Cones were almost entirely depleted by the 1,9-DDF treatment but remained virtually unaffected by the FCCP treatment. Rods, however, were strongly and highly selectively affected by Shikonin and FCCP, while the *no* RPE condition had a relatively minor effect. These results highlight important differences between rod and cone energy metabolism.

Experimental retinal interventions produce characteristic metabolomic patterns

We employed high-field (600 MHz) ^{1}H-NMR spectroscopy-based metabolomics to study the metabolic signatures in the five experimental groups (Supplementary Table 1, Supplementary Figure 3). A principal component analysis (PCA) showed clear group separation (Figure 1I). Unbiased clustering of metabolite profiles revealed specific groups that were differentiated among the five experimental situations (Figure 2A). The greatest cluster overlap was seen in control and Shikonin groups. Significant clustering was observed in several amino acid sub-classes and energy metabolites. We found the strongest changes in

153 the 1,9-DDF condition, where glutamate, aspartate, alanine, O-phosphocholine, and nicotinamide adenine
154 dinucleotide (NAD^+) concentrations were particularly upregulated compared to control. Further,
155 branched-chain amino acids (BCAAs), lactate, and threonine were upregulated in the FCCP and *no* RPE
156 condition. Glutathione (GSH) and glutathione disulfide (GSSG) were relatively reduced by Shikonin
157 treatment, with increased creatine and formate. Control and 1,9-DDF treatment displayed high levels of
158 guanosine triphosphate (GTP), adenosine triphosphate (ATP), and π-methylhistidine, which were low in
159 the other groups (Figure 2A).

160 We then compared metabolite patterns for each treatment to control (Figure 2B). Metabolites were
161 grouped according to class and function, including fundamental metabolic pathways, such as energy and
162 cofactor metabolism, coenzymes, Krebs-cycle, neuronal tissue-associated metabolites and
163 neurotransmitters, BCAAs, glucogenic and ketogenic amino acids (AAs), serine synthesis pathway, cell
164 membrane synthesis, and individual features from redox metabolism.

165 To get an overall impression of treatment effects on energy metabolism, we assessed the adenylate
166 energy charge of the retina under the various experimental conditions and the ratio of GSH to GSSG to
167 investigate oxidative/reductive stress. The energy charge appeared to be reduced in the shikonin and
168 FCCP condition, while the GSH/GSSG ratio of the tissue was not significantly changed from control in any
169 condition (Supplementary Figure 4A, B). We then analyzed the spent culture medium at P15 to assess
170 retinal glucose consumption and lactate production after two days of culture. As could be expected, 1,9-
171 DDF treatment reduced glucose consumption compared to control, while FCCP treatment increased
172 glucose expenditure (Supplementary Figure 4C). Conversely, lactate production was decreased in the 1,9-
173 DDF group. However, in the *no* RPE condition and after FCCP treatment lactate concentrations in the
174 spent medium were strongly and significantly elevated (Supplementary Figure 4D).

175 Afterwards, the metabolomic differences identified within the retina were explored in detail and related
176 to the retinal expression of corresponding enzymes.

177

178 **Retina cultured without RPE displays strongly increased glycolytic activity**

179 The RPE is tightly bound to the choroid and serves as interface between vasculature and neuroretina.
180 Because of the strong adherence of RPE to the choroid, most prior studies on explanted retina were
181 performed without RPE (4, 11). To understand the metabolic communication between neuroretina and
182 RPE, we prepared organotypic retinal explants both with RPE (control) or without RPE (*no* RPE). Since
183 most previous studies on retinal energy metabolism had used retina without RPE (4, 23), this comparison
184 also allowed us to relate our data to those earlier results.

185 The metabolite profile of control was markedly different from retina cultured without RPE, with 25
186 metabolites exhibiting significant changes (Figure 3A, Supplementary Figure 5). Decreased ATP levels in
187 the *no* RPE group, corresponded to increased lactate. The BCAAs isoleucine, leucine, and valine, and some
188 of the glucogenic/ketogenic AAs threonine, methionine, glycine, displayed higher levels in the *no* RPE
189 group compared to control. Alanine, aspartate, and taurine showed the opposite trend. Hypotaurine, 4-
190 aminobutyrate (GABA), and glutamate were accumulated in retinal tissue, while membrane synthesis-
191 associated metabolites, such as myo-inositol and O-phosphocholine, as well as creatine and N-
192 acetylaspartate (NAA) were reduced in neuroretina. Moreover, higher levels of GSSG appeared in the
193 absence of RPE, pointing towards an altered redox metabolism.

194 Pattern hunter (Pearson R) correlation analysis found citrate, a central Krebs-cycle metabolite, positively
195 correlated with taurine, alanine, aspartate, and ATP (Figure 3B). Negative correlations with citrate
196 included ADP, BCAAs, and lactate. A subsequent KEGG-based pathway analysis revealed changes in
197 arginine and proline metabolism, taurine and hypotaurine metabolism, and alanine, aspartate, and
198 glutamate metabolism in the *no* RPE situation (Figure 3C).

199 Immunofluorescence was used to localize enzymes likely responsible for the observed metabolic changes
200 (Figure 3D). Citrate synthase (CS) and fumarase, key enzymes of the Krebs-cycle, were found mostly in
201 photoreceptor inner segments and synaptic terminals. The γ-subunit of ATP synthase, essential for
202 OXPHOS, was also localized to photoreceptor inner segments and synapses. Thus, low ATP levels in the *no*
203 RPE group likely resulted from decreased photoreceptor Krebs-cycle and OXPHOS activity. High levels of
204 taurine were detected in photoreceptor inner segments and synapses, as well as in the ganglion cell layer
205 (Figure 3D). Finally, the enzyme alanine transaminase (ALT), previously thought to be expressed only in
206 muscle and liver, was found to be expressed in the inner nuclear and plexiform layers (Figure 3D). ALT was
207 also strongly expressed in cone inner segments, as evidenced by co-labelling with cone-Arr3. This
208 expression pattern and high alanine levels in the control strongly suggested Cahill-cycle activity in the
209 retina (14). When ALT activity was inhibited with β-chloro-alanine, photoreceptor cell death was
210 increased and notably cone survival was reduced, functionally validating the expression of ALT in the
211 outer retina (Supplementary Figure 6A, B).

212 The patterns observed in the *no* RPE to control comparison indicated that retinal metabolism strongly
213 depended on RPE-to-neuroretina interactions, including shuttling of metabolites such as
214 hypotaurine/taurine. Notably, the accumulation of BCAA, glutamate, and lactate, concomitant with
215 decreased alanine levels in the *no* RPE group, implied that RPE removal switched retinal metabolism from
216 Krebs-cycle/OXPHOS to aerobic glycolysis.

217

218 **Photoreceptors use the Krebs-cycle to produce GTP**

219 Since in Figure 2, the *no* RPE and FCCP groups showed similar metabolite patterns and pathway changes
220 overall, we subjected these two experimental groups to a detailed statistical analysis. This revealed 17
221 significant metabolite changes (Figure 4A; Supplementary Figure 7). Among the most highly reduced
222 metabolite concentrations in the FCCP group was GTP, which positively correlated with GABA, ATP, GSSG,
223 hypotaurine, and NAD^+ (Figure 4B). In contrast, GDP, BCAAs, glutamine, and citrate negatively correlated
224 to GTP. The KEGG-based pathway analysis ranked glycine, serine and threonine metabolism, glutathione
225 metabolism, and alanine, aspartate and glutamate metabolism as the most significantly changed between
226 the two conditions (Figure 4C).

227 Curiously, measurable amounts of GTP can only be generated in two ways: 1) by succinate-CoA ligase,
228 GTP-forming-1 (SUCLG-1) in the Krebs-cycle, and 2) from excess ATP by nucleoside-diphosphate kinase
229 (NDK) an enzyme expressed in photoreceptor inner and outer segments (24, 25). Since ATP levels were
230 low in both the FCCP and the *no* RPE situation, here, GTP could not have been produced from ATP.
231 Immunofluorescence for SUCLG-1 showed strong expression in photoreceptor inner segments and
232 synapses, where it co-localized to a large extent with mitochondrial COX (Figure 4D). Hence, the SUCLG-1
233 retinal expression pattern and the synthesis of GTP in the absence of RPE provided clear evidence for
234 Krebs-cycle activity in photoreceptors.

235 We also identified an FCCP-induced upregulation of citrate, concomitant with a downregulation of NAD^+.
236 This indicated a Krebs-cycle interruption at the level of D-isocitrate to α-ketoglutarate conversion, *i.e.*, a
237 step that requires NAD^+. NAD^+ is known to be consumed by poly-ADP-ribose-polymerase (PARP), which is
238 activated by oxidative DNA damage (26) and up-regulated in dying photoreceptors (27). Therefore, we
239 quantified poly-ADP-ribose (PAR) accumulation in retinal cells as a marker for PARP activity. Compared to
240 the *no* RPE group, more photoreceptor cells in the FCCP-treated retina showed PAR accumulation,
241 correlating with decreased retinal NAD^+ levels (Figure 4E, F). Hence, FCCP-induced oxidative stress may
242 cause increased PARP activity and decreased NAD^+ levels, eventually interrupting the Krebs-cycle, as
243 evidenced by citrate accumulation.

244 Overall, the data from the *no* RPE to FCCP group comparison showed that disruption of OXPHOS led to AA
245 accumulation, including lysine, phenylalanine, glutamine, leucine, and valine. Notably, alanine

246 accumulation in the FCCP group was likely caused by ALT-dependent pyruvate transamination. By
247 contrast, metabolites high in the *no RPE* group but low with FCCP treatment were probably related to
248 Krebs-cycle in the neuroretina. This concerned especially GTP, aspartate, and NAA.

249

250 **Reduced retinal glucose uptake promotes anaplerotic metabolism**

251 Since GLUT1 was predominantly expressed in the RPE, we initially assumed that the metabolic response
252 to 1,9-DDF treatment might resemble that of the *no* RPE situation. However, the patterns found between
253 these two groups were very different (*cf.* Figure 2) and to explore these differences further, we performed
254 an additional two-way comparison. This analysis revealed 28 significantly changed metabolites (Figure 5A;
255 Supplementary Figure 8). When compared to the *no* RPE, the 1,9-DDF group showed changes in
256 mitochondria and Krebs-cycle-associated metabolites (*e.g.*, high ATP, high formate, low BCAA).
257 Conversely, the Cahill-cycle product alanine and NAA were upregulated by 1,9-DDF treatment. The
258 pattern hunter analysis showed that metabolites formate, glutamate, taurine, and citrate were positively
259 correlated with ATP, while, AMP, GMP, and BCAA were negatively correlated with ATP (Figure 5B).

260 The KEGG pathway analysis showed alanine, aspartate, and glutamate metabolism, glutathione
261 metabolism and glycine, serine, and threonine metabolism among the three most affected pathways
262 (Supplementary Figure 8B). Taken together, the depletion of BCAAs in the 1,9-DDF treatment indicated
263 that either the RPE, the neuroretina, or both used anaplerotic substrates to fuel the Krebs-cycle and
264 maintain ATP production.

265

266 **Inhibition of glycolysis strongly impacts retinal ATP production**

267 Next, we compared the Shikonin treatment, which inhibits the last step of glycolysis, to the FCCP
268 treatment, which abolishes mitochondrial ATP synthesis, *i.e.* we compared two experimental situations
269 that could be seen as manipulations of the two opposing ends of energy metabolism, non-oxidative
270 glycolysis and OXPHOS. This analysis showed increased formate, aspartate, and NAA levels in the Shikonin
271 group (Figure 5C). Conversely, higher amounts of GSH, GSSG, BCAA, threonine, and phenylalanine after
272 FCCP treatment indicated Krebs-cycle interruption (Supplementary Figure 9). The production of lactate
273 was higher with FCCP- compared to Shikonin treatment, probably reflecting increased glycolysis to
274 compensate for the loss of Krebs-cycle-dependent ATP production. Metabolites connected to oxidative
275 stress, such as GSSG and GSH, were also increased by FCCP treatment. Pattern hunter for metabolites
276 correlated with glutathione found 3-hydroxyisovalerate, glutamine, GSSG, but also lactate and ATP, while
277 succinate, alanine, and GABA were negatively correlated with GSH (Figure 5D). The subsequent pathway
278 analysis identified arginine biosynthesis, alanine, aspartate, and glutamate metabolism, as well as
279 glycolysis and gluconeogenesis as the most strongly regulated metabolic pathways (Supplementary Figure
280 9B).

281

282 **Blocking glucose uptake and OXPHOS disruption reveal distinct rod and cone metabolism**

283 The metabolic rate of cones is at least two times higher than that of rods (9). The treatment with 1,9-DDF
284 resulted in near complete cone loss, while cones were fully preserved with FCCP treatment (*cf.* Figure 1).
285 Although we did not expect these differential treatment effects on cone survival, we used this outcome in
286 an explorative approach to try and investigate the relative contributions of rods and cones to the
287 metabolite patterns observed.

288 In this three-way comparison, 29 metabolite concentrations were significantly changed (Figure 6A;
289 Supplementary Figure 10). The FCCP treatment reduced ATP and GTP levels, while lactate production was
290 greatly increased, along with methionine and threonine. BCAAs, glutamine, phenylalanine and tyrosine

also showed a significant upregulation with FCCP treatment. Interestingly, some metabolites like GSSG, serine, glutamate, alanine, NAD^+, and taurine displayed a pronounced increase in the 1,9-DDF group when compared to either control or FCCP. In addition, formate, aspartate, and myo-inositol were upregulated with 1,9-DDF treatment, together with NAA and creatine. Finally, the comparison between the 1,9-DDF and FCCP groups revealed highly increased levels of ATP and GTP, implying a strong activation of the Krebs-cycle under 1,9-DDF treatment.

A cell type-specific attribution of these metabolite patterns may be superseded by direct drug treatment effects. Using only metabolite changes in opposing directions from control to interpret different cellular compositions, we identified BCAAs, tyrosine, NAA, and ATP (Supplementary Figure 10). BCAAs and tyrosine (and glutamine) exhibited low levels in the rod-rich 1,9-DDF group and high levels in the cone-rich FCCP group, indicating that these metabolites might be consumed by rods or produced in cones. Vice versa, it may be assumed that aspartate and NAA were predominantly produced in rods.

To investigate the role of glutamine in retinal metabolism, we used immunofluorescence (Figure 6B). We confirmed a strong expression of glutamine synthase (GS) in MGCs (28). Remarkably, the enzyme that hydrolyses glutamine to glutamate, glutaminase C (GAC) was prominently expressed in photoreceptor inner segments, photoreceptor synapses, and INL. Co-labelling with cone Arr3 revealed a strong expression of GAC in cone inner segments, implying that cones could use glutamine as a metabolic substrate. Accordingly, treatment with the GAC-specific inhibitor Compound 968 dose-dependently reduced photoreceptor viability – affecting cones more strongly than rods – while leaving the inner retina mostly intact (Supplementary Figure 6C, D).

Impact on glycolytic activity, serine synthesis pathway, and anaplerotic metabolism

To assess how the various experimental interventions affected retinal metabolism, we calculated the ratios for pathway-specific metabolites (Figure 6C). GTP, when produced by SUCLG-1, is a marker for Krebs-cycle activity, while lactate indicates glycolytic activity. In the *no* RPE group, the GTP-to-lactate ratio was significantly lower than in control, indicating 4.1-times higher glycolytic activity. While in the 1,9-DDF and Shikonin group the GTP-to-lactate ratios were not significantly different from control, with FCCP treatment this ratio dropped to the lowest level, in line with a strong downregulation of Krebs-cycle and concomitant upregulation of glycolysis.

We then calculated the ratio of serine to lactate as an indicator for serine synthesis pathway activity. Under control conditions, and in the *no* RPE and FCCP groups, this activity was rather low, while it was strongly increased by 1,9-DDF and Shikonin treatment. In the Shikonin group, serine production from 3-phosphoglycerate and subsequent deamination to pyruvate may bypass the PKM2 block. Serine is also a precursor of phosphatidylserine, one of the three main cell membrane components. Together with a reduction of choline and high concentrations of myo-inositol, O-phosphocholine, and O-phosphoethanolamine, this may reflect high cell membrane synthesis under 1,9-DDF treatment.

Finally, we used the ratio of GTP to BCAAs to investigate to what extent Krebs-cycle activity was driven by anaplerotic metabolism. A comparatively low GTP to BCAA ratio in the *no* RPE situation showed that much of the GTP generated in the neuroretina likely came from anaplerotic substrates. While both Shikonin and FCCP treatment decreased BCAA use, 1,9-DDF treatment increased anaplerotic metabolism.

Evidence for mini-Krebs-cycle activity

Comparing the ratios of GTP to lactate with GTP to BCAA in the *no* RPE situation showed that a large proportion of the GTP produced in the neuroretina by SUCLG-1 was derived from anaplerotic substrates rather than from pyruvate. These substrates enter the Krebs-cycle mostly at the level of α-ketoglutarate, suggesting that the neuro-retinal Krebs-cycle might not start with citrate. Instead, only an α-ketoglutarate

337 to oxaloacetate shunt would be employed, including the GTP-synthesizing step from succinyl-CoA to
338 succinate (Figure 7A). A key step of this mini-Krebs-cycle (28) is the transamination of oxaloacetate with
339 glutamate by aspartate aminotransferase (AST) to yield α-ketoglutarate and aspartate, which is further
340 acetylated to NAA. To investigate this possibility, we analyzed eight metabolites associated with the
341 Krebs-cycle (citrate, succinate, fumarate, GTP) and the hypothesized mini-Krebs-cycle (glutamine,
342 glutamate, aspartate, NAA).

343 Hierarchical clustering showed similar patterns for aspartate and NAA in all experimental conditions
344 (Figure 7B). Except for the FCCP treatment, the ratio of citrate/NAA was 0.5, indicating that the retina
345 preferred the mini-Krebs-cycle over the full Krebs-cycle (Figure 7C). Immunolabelling for AST –
346 conventionally associated with muscle and liver metabolism (29, 30) – found both AST1 and AST2 to be
347 expressed in photoreceptor inner segments and cell bodies (Figure 7D). This confirmed that
348 photoreceptors can execute the mini-Krebs-cycle, while the NAA production seen in the metabolomic
349 data suggested that this cycle was indeed used.

350 Finally, we compared the energetic efficiencies of glycolysis, Krebs, Cori, Cahill, and mini-Krebs cycle
351 (Figure 8). Using anaplerotic substrates the Cahill- and mini-Krebs cycles allow for far more efficient
352 energy production compared to the Cori-cycle. Moreover, mitochondrial PCK2 can regenerate pyruvate
353 from oxaloacetate. Assuming that one mole of NADH/$FADH_2$ can be used to generate three moles of ATP
354 via OXPHOS, and depending on the exact stoichiometry of glutamate/BCAA input, the mini-Krebs-cycle
355 may deliver up to 18 moles of ATP and 2 moles of GTP per 3 carbon unit. Astonishingly, this exceeds the
356 15 moles of ATP and 1 mole of GTP generated in the "full" Krebs-cycle.

357

358 ## Discussion

359 This study combined cellular enzyme expression patterns with quantitative metabolomics of retinal
360 explants. In an entirely controlled environment, this enabled a comprehensive assessment of retinal
361 metabolism and enabled an analysis of the impact of different experimental conditions on retinal cell
362 death and survival. As opposed to earlier works, our study highlights the crucial importance of OXPHOS
363 and anaplerotic pathways for the maintenance and survival of rod and cone photoreceptors. Importantly,
364 we show that photoreceptors are able to uncouple glycolysis and Krebs-cycle using a NAA-producing
365 shunt. This allows the use of both pathways in parallel and may resolve a long-standing problem in
366 neuronal energy metabolism research. Because of the ramifications for overall cellular physiology, these
367 findings are highly relevant for future therapy developments, for retinal diseases, as well as for
368 neurodegenerative and further metabolic diseases in general.

369

370 ### The retina as an experimental system for studies into neuronal energy metabolism

371 The study of neuronal metabolism in a living mammalian is notoriously difficult as there is constant
372 interaction between different subcellular compartments, cell types, tissues, and organs (31). The retina
373 may be a special case as it can function in isolation, *e.g.* as in an explant (32), which is why many prior
374 studies on retinal metabolism employed explanted retina. However, in most retinal explant preparations
375 the RPE separates from the neuroretina. Such explants were used in Otto Warburg´s seminal studies in
376 the 1920s, where the retina was found to release large amounts of lactate (4). Later studies by Barry
377 Winkler, using a similar experimental setup namely explanted rat retina without RPE (23), confirmed
378 Warburg´s original work and expanded on the idea that the neuroretina was using aerobic glycolysis.

379 *In vivo* studies on retinal metabolism are significantly more challenging and hence relatively rare. For
380 example, in cats, the blood lactate concentration, sampled via choroidal vein cannulation, was compared
381 against femoral artery lactate levels, concluding that a major fraction of retinal glucose was used for
382 aerobic glycolysis (33). In contrast, monkey *in vivo* micro-electrode measurements indicated major oxygen

383 consumption in photoreceptor inner segments, implying the use of OXPHOS (34). Future more
384 comprehensive *in vivo* studies of retinal metabolism may require the simultaneous cannulation of central
385 retinal artery and central retinal vein, combined with oxygen-sensing and metabolomic analysis. Such
386 experiments may need to employ larger animal species (*e.g.* dog, monkey) to overcome limitations in eye
387 and blood sample size.

388 Our *in vitro* approach may be seen as a compromise between earlier *in vitro* studies and the *in vivo*
389 situation. Organotypic retinal explants maintain the histotypic context of the tissue, the interactions
390 between its various cell types, full functionality and light responsiveness, and are cultured under defined
391 conditions, devoid of serum and antibiotics (32, 35). These retinal explants are derived from early post-
392 natal retina (day 9) and can be cultured for up to six weeks *in vitro* without major cell loss (36).
393 Importantly, our retinal explant cultures include the RPE (except for the *no* RPE condition) and may thus
394 be closer to the *in vivo* situation than previous *in vitro* studies. While the combination of this *in vitro*
395 approach with ^{1}H-NMR metabolomics can be very powerful, it assumes that mainly photoreceptors are
396 responsible for changes in retinal metabolism. Given the large photoreceptor energy consumption (5, 11)
397 this assumption may often be correct, yet caution is warranted to not miss metabolic responses of smaller
398 cell populations (*e.g.* Müller glia, RPE cells).

399

400 **Photoreceptors may use both glucose and anaplerotic substrates as fuel**

401 Under anaerobic conditions, the production of lactate from glucose is a hallmark of skeletal muscle
402 function. Here, pyruvate is reduced to lactate, which enters the bloodstream to serve as substrate for liver
403 gluconeogenesis. Glucose can then be cycled back to the muscle. This glucose-lactate cycle between
404 muscle and liver was discovered in the 1930s and is referred to as Cori-cycle (12). The release of large
405 amounts of lactate from isolated retina suggested that also the retina might use the Cori-cycle, albeit
406 under aerobic conditions (37). Photoreceptors have thus been proposed to consume primarily glucose via
407 aerobic glycolysis (11). The resultant lactate would be used as fuel in the Krebs-cycle by RPE and MGCs,
408 generating ATP via OXPHOS. However, this hypothesis is contradicted by the high density of mitochondria
409 in photoreceptor inner segments (38). Moreover, key enzymes for Krebs-cycle (CS, FH, SUCLG1) and
410 OXPHOS (COX, ATP synthase γ) were strongly expressed in photoreceptors, but showed little or no
411 expression in RPE or MGCs, in line with previous research (25). When we cultured retina without RPE, as
412 done by Warburg and others (4, 11), we indeed confirmed a strong lactate production. Yet, in retina
413 cultured with RPE, lactate production was minor. Moreover, retina without RPE still produced large
414 amounts of GTP, likely stemming from SUCLG1 activity and indicating Krebs-cycle operation in
415 photoreceptors. Neuroretina without RPE displayed reduced viability of both rod and cone
416 photoreceptors, as well as an accumulation of BCAAs and lactate. In contrast, the block of glucose import
417 into the RPE by treatment with 1,9-DDF (39) resulted in a depletion of BCAAs and other AAs, and an
418 increase of retinal ATP, indicating a switch from glycolytic to anaplerotic metabolism (15). This is in line
419 with an earlier study using a conditional GLUT1 knockout in the RPE, which yielded evidence for a
420 compensatory upregulation of anaplerotic metabolism in photoreceptors (3). Hence, photoreceptors
421 likely consume both glucose and anaplerotic substrates as fuels, with retinal metabolism switching to
422 aerobic glycolysis only in the absence of RPE. This switch may be driven by increased glucose uptake.

423 In intact retina, tight junction-coupled RPE cells form the outer blood-retinal barrier and prevent direct
424 access of glucose to photoreceptors (40). In the absence of RPE, photoreceptors expressing the high
425 affinity/high capacity GLUT3 become "flooded" with glucose. The resultant Crabtree effect likely causes a
426 shutdown of Krebs-cycle activity (18, 41, 42), effectively starving photoreceptors to death because a
427 purely glycolytic metabolism may not generate sufficient ATP for their survival. As seen in the *no* RPE
428 group, cones appear to be more sensitive to this effect, perhaps because their overall energy demand is
429 twice as high as that of rods (9). Surprisingly, FCCP treatment did not reduce cone viability suggesting that
430 for cones high glucose is more toxic than a lack of OXPHOS. At any rate, it is probably the lack of the

431 blood-retinal barrier function that leads to the strong differences in metabolite patterns seen between
432 the 1,9-DDF treatment and the *no* RPE group. Taken together, the high rates of retinal aerobic glycolysis
433 first reported by Otto Warburg are likely an artefact of the absence of RPE, while intact retina may rely
434 more on OXPHOS for its energy production.

435

436 **Rods need OXPHOS, cones need glycolysis**

437 Treatment with FCCP revealed striking differences between rod and cone energy metabolism. FCCP
438 eliminates the proton gradient between inner mitochondrial membrane and mitochondrial matrix,
439 abolishing ATP synthesis (43). Initially, FCCP may increase Krebs-cycle activity to attempt restoration of
440 mitochondrial proton gradient (44), increasing oxidative stress (45), and oxidative DNA damage. The
441 resultant activation of PARP would deplete NAD^+, further aggravating metabolic stress (46). Although
442 FCCP had a strong toxic effect on rod photoreceptors, remarkably, cone photoreceptors were almost
443 completely preserved. Theoretically, it is conceivable that FCCP primarily affected the RPE and that
444 photoreceptor degeneration occurred secondarily to that. However, then, rods and cones would likely
445 have been equally affected by FCCP treatment. In striking contrast to the FCCP effect was that of the 1,9-
446 DDF block on GLUT1 (39). Although GLUT1 was strongly expressed in the RPE, glucose entering the RPE is
447 shuttled forward to photoreceptors (3). Remarkably, with 1,9-DDF, over 90 % of cones were lost, while
448 the detrimental effect on rods was comparatively minor. These differential effects of FCCP and 1,9-DDF
449 treatments strongly suggest that glycolysis is sufficient and necessary for cone survival, in agreement with
450 earlier studies who showed that under stress cones require glycolysis to remain viable (47, 48).

451 Conversely, rods require OXPHOS for their survival, while glycolysis is of minor importance. Furthermore,
452 cone viability relative to rods was also strongly compromised in the *no* RPE situation, indicating that an
453 intact blood-retinal barrier (40) and regulation of glucose access was important for cone survival. Future
454 studies analyzing specific mouse mutants which have either only rods (*e.g.* the *cpfl1* mouse (49) or only
455 cones (*e.g.* the NRL knock-out mouse (50) may give more detailed insights into rod and cone metabolism.

456

457 **Expression of glucose transporters in the outer retina**

458 Our work shows that RPE cells express high levels of GLUT1, while photoreceptors express the neuronal
459 glucose transporter GLUT3. Furthermore, GLUT2 may contribute to photoreceptor glucose uptake
460 indirectly via horizontal cells (51). We note that there is a controversy in the literature regarding the
461 expression of GLUT1 on photoreceptors. Although there seems to be a general agreement that GLUT1 is
462 expressed on RPE cells (3), several studies have suggested GLUT1 expression also on photoreceptors, both
463 on rods and cones (48, 52) In the brain the generally accepted setup for GLUT1 and GLUT3 expression is
464 that low-affinity GLUT1 (Km = 6.9 mM) is expressed on glial cells, which contact blood vessels, while high-
465 affinity GLUT3 (Km = 1.8 mM) is expressed on neurons (53, 54). This setup matches decreasing glucose
466 concentration with increasing transporter affinity, for an efficient transport of glucose from blood vessels
467 to glial cells to neurons. In the retina, the cells that contact the choroidal blood vessels are the tight-
468 junction-coupled RPE cells. Since RPE cells express GLUT1, an efficient glucose transport from the RPE to
469 the energy-hungry photoreceptors, requires photoreceptors to express a glucose transporter with a
470 glucose affinity higher than GLUT1. Our finding of GLUT3 expression on photoreceptors matches this
471 requirement. Still, at this point we cannot exclude a low level expression of GLUT1 on other retinal cell
472 types, for instance on Müller glia cells (55) which might use GLUT1 to export excess glucose resulting from
473 gluconeogenesis (56) Moreover, there are 10 further glucose transporters, some of which might be
474 expressed in the retina. A comprehensive study of the retinal protein expression of all glucose
475 transporters, using, for example, CODEX technology (57), may reveal their expression patterns and
476 putative functions in the future.

477

478 **Cone photoreceptors likely employ the Cahill-cycle**

479 The lactate-generating Cori-cycle (12) is highly inefficient and in intact retina likely plays a lesser role. An
480 efficient pathway is the glucose-alanine cycle, or Cahill-cycle, in which pyruvate, instead of being reduced
481 to lactate, is transaminated to alanine (14). This preserves NADH and generates α-keto acids to fuel the
482 Krebs-cycle. The alanine generated enters the bloodstream and is taken up by the liver, where the
483 ammonia is excreted in the form of urea, while the carbon backbone is used for gluconeogenesis. The key
484 enzyme for the Cahill-cycle is ALT, conventionally associated with muscle and liver function (29, 30).
485 Previously, ALT was found in glial cells of the honeybee retina (44), and ALT activity was detected in rat
486 retinal tissue lysates (58). In our study, the localization of ALT in photoreceptors and inner retinal
487 neurons, combined with our interventional and metabolomic datasets, provided evidence for the
488 operation of the Cahill-cycle in the mammalian retina. Moreover, the expression of mitochondrial PCK2 in
489 cones facilitates the efficient uncoupling of glycolysis from the Krebs-cycle, suggesting that cones may use
490 the Cahill-cycle for very effective energy production.

491

492 **Glutamine from MGCs may provide additional fuel for cones**

493 MGCs are known for their uptake of extracellular glutamate and use for glutamine synthesis. In fact, in
494 retinal histology, glutamate-aspartate transporter (GLAST) and glutamine synthase (GS) have been widely
495 used as markers for MGCs (25, 28). Glutaminase C (GAC) converts glutamine back to glutamate, which
496 could then serve as a substrate for the mini-Krebs-cycle. We localized GAC in inner retinal neurons and
497 photoreceptors, with a particularly strong expression in cone inner segments. Here, GAC overlapped with
498 ALT expression, indicating that cones can use glutaminolysis to obtain extra glutamate for pyruvate
499 transamination in the Cahill-cycle. This may also explain why the glycolysis inhibitor Shikonin reduced
500 cone viability much less than that of rods. In this situation, cones might be able to use the serine-synthesis
501 pathway – with serine production from 3-phosphoglycerate and subsequent deamination to pyruvate – to
502 bypass the Shikonin block of PKM2.

503

504 **A hypotaurine-taurine shuttle can transfer NADH from RPE to photoreceptors**

505 The regeneration of the photoreceptor photopigment retinal is performed by the RPE (16). Recently,
506 retinal has been proposed to form a Schiff base adduct with taurine, which would act as a retinal carrier
507 and buffer (59). Moreover, taurine has been suggested to be an important osmolyte in the retina that
508 may flow in and out of neuronal cells in response to neuronal activity (60, 61).

509 We found that retina cultured with RPE harbored high levels of taurine and low levels of hypotaurine,
510 while retina without RPE displayed low levels of taurine and high levels of hypotaurine. Our taurine
511 immunostaining found essentially no taurine in the RPE, while photoreceptor inner segments and
512 synapses displayed very high taurine levels. Together, these findings suggest a hypotaurine-taurine
513 shuttle between RPE and photoreceptors. In the RPE taurine can be reduced to hypotaurine and shuttled
514 back to photoreceptors where oxidation by hypotaurine dehydrogenase (59, 62) may reconstitute taurine,
515 yielding additional NADH for OXPHOS. The net effect of this hypotaurine-taurine shuttle would be a
516 transfer of reducing power from RPE to photoreceptors, boosting photoreceptor ATP production via
517 OXPHOS. In addition, it seems likely that hypotaurine-taurine shuttling will have an impact on the
518 osmolarity of both photoreceptors and RPE cells.

519

520 **Rods can use the mini-Krebs-cycle to uncouple glycolysis from mitochondrial metabolism**

521 A key problem in the understanding of cellular energy metabolism is the relationship between fast but
522 inefficient glycolysis and slow but efficient Krebs-cycle/OXPHOS (63, 64). Both pathways are coupled via

523 pyruvate and the different metabolic flow rates reduce the efficiency of energy production, *e.g.*, via
524 feedback inhibition (65). Pyruvate coupling is especially problematic in high and rapidly changing energy
525 demand such as in neurons and photoreceptors (66). Uncoupling glycolysis and Krebs-cycle via the Cori-
526 cycle is extremely wasteful and likely insufficient to satisfy long-term photoreceptor energy demand. By
527 comparison, the Cahill-cycle delivers additional NADH when using pyruvate derived from glycolysis, and
528 cones may use the Cahill-cycle for uncoupling from glycolysis.

529 An alternative pathway is the mini-Krebs-cycle, essentially an oxalacetate to α-ketoglutarate shunt (15).
530 This cycle uses glutamate, glutamine, and BCAAs as fuels to run mitochondrial respiration independent of
531 glycolysis. The key step of the mini-Krebs-cycle is the transamination of oxaloacetate/glutamate to
532 aspartate/α-ketoglutarate by AST. α-Ketoglutarate is then metabolized to oxaloacetate, generating NADH,
533 $FADH_2$, and GTP. Acetyl-CoA generated from BCAAs or pyruvate is used to create NAA, the end product of
534 the mini-Krebs-cycle. We found mitochondrial AST2 to be expressed in rod inner segments, in agreement
535 with an early cytochemical study (67). This indicates that the mini-Krebs-cycle is used primarily by rods,
536 perhaps explaining their selective vulnerability to FCCP treatment. Crucially, the mini-Krebs-cycle is more
537 energy-efficient than the Cahill-cycle and generates NAA instead of alanine as net product. Both
538 metabolites serve the purpose of disposing of excess ammonia originating from AA input (68, 69). NAA in
539 the human brain is one of the most abundant metabolites and is routinely used in clinical MRI diagnosis to
540 visualize brain health (70). While different functions have been hypothesized for NAA (71, 72), our work
541 proposes NAA as a signature metabolite for the mini-Krebs-cycle. Indeed, a recent study using Raman
542 spectroscopy imaging detected high levels of NAA in the human retina, demonstrating *in vivo* use of this
543 cycle (73). Importantly, the 6-step mini-Krebs-cycle is significantly faster than the 10-step Krebs-cycle (15),
544 more energy-efficient, and uncoupled from glycolysis. While the high metabolic rate of photoreceptors
545 suggests that mini-Krebs-cycle metabolites will mostly originate there, the strong AST1/AST2 expression
546 observed in the inner plexiform layer suggests that the mini-Krebs-cycle may also play a role in fueling
547 synaptic activity. Moreover, in rods, PCK1 may allow to replenish cytoplasmic acetyl-CoA pools from
548 oxaloacetate, if BCAA-derived input was insufficient.

549 In the future, it will be very interesting to perform carbon- or nitrogen tracing studies using ^{13}C-or ^{15}N-
550 labelled alternative fuels, including glucose, lactate, and glutamate/glutamine, to measure which
551 metabolites are produced under what experimental conditions. Such tracing studies would also allow to
552 establish the flux of metabolites through a specific pathway, something that is difficult to assess with our
553 current steady-state measurements.

554 Overall, the different pathways outlined here provide photoreceptor cells with remarkable versatility and
555 flexibility in terms of substrate use, enabling them to dynamically adapt the timing and quantitative
556 output of energy metabolism. Rods rely strongly on the Krebs-cycle and OXPHOS, while cones are more
557 dependent on glycolysis. These differences between rod and cone metabolism may be related to their
558 response kinetics and sensitivities. The flexible uncoupling of glycolysis from mitochondrial respiration,
559 allows both processes to run at optimum, producing the characteristic signature metabolites lactate (Cori-
560 cycle), alanine (Cahill-cycle), and NAA (mini-Krebs-cycle). These metabolites can reveal energy or disease
561 status and could serve as readout and guide for the design of novel therapeutic interventions. Given the
562 general importance of energy metabolism, the significance of our findings extends beyond the retina, for
563 instance, to other neurodegenerative and metabolic diseases.

564

Materials and Methods

C3H wild-type (WT) mice were used to generate organotypic retinal explant cultures (18). All efforts were made to minimize the number of animals used and their suffering. For details on the experimental procedures, immunofluorescence, and antibodies, as well as metabolomic analysis and databases used please refer to the supporting information (SI).

Declarations

Ethics approval and consent to participate

Protocols compliant with the German law on animal protection were reviewed and approved by the institution for animal welfare, veterinary service and laboratory animal science (Einrichtung für Tierschutz, Tierärztlichen Dienst und Labortierkunde) of the University of Tübingen and were following the association for research in vision and ophthalmology (ARVO) statement for the use of animals in vision research.

Availability of data and materials

Raw NMR spectroscopy data is available upon request. Any additional information required to reanalyze the data reported in this paper is available from the lead contact upon request. This paper does not report original code.

Competing interests

The authors declare no competing financial interests. CT reports a research grant by Bruker BioSpin GmbH.

Funding

This work was funded by the ProRetina Foundation, the Zinke heritage foundation, the Werner Siemens Foundation, the Chinese scholarship council (CSC), ANID-FONDECYT No. 1210790 (OS) and PhD grant BECAS CHILE/2018 -21180443 (VC). We also acknowledge support from the Open Access Publication Fund of the University of Tübingen.

CRediT author contribution statement

Yiyi Chen: Conceptualization, Methodology, Investigation, Writing – original draft. **Laimdota Zizmare**: Conceptualization, Methodology, Investigation, Writing – original draft, Writing – Review & Editing. **François Paquet-Durand**: Conceptualization, Methodology, Investigation, Writing – original draft, Writing – Review & Editing, Supervision, Funding acquisition. **Christoph Trautwein**: Conceptualization, Methodology, Investigation, Writing – original draft, Writing – Review & Editing, Supervision, Funding acquisition. **Shirley Yu**: Investigation. **Lan Wang**: Investigation. **Friedrich W. Herberg**: Writing – Review & Editing. **Oliver Schmachtenberg**: Writing – Review & Editing. **Victor Calbiague**: Writing – Review & Editing.

Acknowledgements

We thank N. Rieger, M. Owczorz, and D. Bucci for first-rate technical support, as well as James B. Hurley and Daniel Hass (both University of Washington, Seattle, USA) for helpful comments and suggestions.

604

605 **References**

606 1. M. W. Country, Retinal metabolism: A comparative look at energetics in the retina. *Brain*
607 *Res* **1672**, 50-57 (2017).
608 2. M. T. Wong-Riley, Energy metabolism of the visual system. *Eye Brain* **2**, 99-116 (2010).
609 3. A. Swarup *et al.*, Modulating GLUT1 expression in retinal pigment epithelium decreases
610 glucose levels in the retina: impact on photoreceptors and Müller glial cells. *Am J Physiol*
611 *Cell Physiol* **316**, C121-c133 (2019).
612 4. O. Warburg, The metabolism of carcinoma cells. *The Journal of Cancer Research* **9**, 148-
613 163 (1925).
614 5. H. Okawa, A. P. Sampath, S. B. Laughlin, G. L. Fain, ATP consumption by mammalian rod
615 photoreceptors in darkness and in light. *Curr Biol* **18**, 1917-1921 (2008).
616 6. A. Ames, 3rd, Energy requirements of CNS cells as related to their function and to their
617 vulnerability to ischemia: a commentary based on studies on retina. *Can J Physiol*
618 *Pharmacol* **70 Suppl**, S158-164 (1992).
619 7. Y. Chinchore, T. Begaj, D. Wu, E. Drokhlyansky, C. L. Cepko, Glycolytic reliance promotes
620 anabolism in photoreceptors. *Elife* **6** (2017).
621 8. R. W. Young, The renewal of photoreceptor cell outer segments. *J Cell Biol* **33**, 61-72
622 (1967).
623 9. N. T. Ingram, G. L. Fain, A. P. Sampath, Elevated energy requirement of cone
624 photoreceptors. *Proceedings of the National Academy of Sciences* **117**, 19599-19603
625 (2020).
626 10. O. Strauss, The retinal pigment epithelium in visual function. *Physiol Rev* **85**, 845-881
627 (2005).
628 11. M. A. Kanow *et al.*, Biochemical adaptations of the retina and retinal pigment epithelium
629 support a metabolic ecosystem in the vertebrate eye. *Elife* **6** (2017).
630 12. C. F. Cori, G. T. Cori, Carbohydrate metabolism. *Annu Rev Biochem* **15**, 193-218 (1946).
631 13. G. F. Cahill, Jr., O. E. Owen, Starvation and survival. *Trans Am Clin Climatol Assoc* **79**, 13-
632 20 (1968).
633 14. P. Felig, The glucose-alanine cycle. *Metabolism* **22**, 179-207 (1973).
634 15. M. Yudkoff, D. Nelson, Y. Daikhin, M. Erecińska, Tricarboxylic acid cycle in rat brain
635 synaptosomes. Fluxes and interactions with aspartate aminotransferase and
636 malate/aspartate shuttle. *J Biol Chem* **269**, 27414-27420 (1994).
637 16. T. M. Redmond *et al.*, Rpe65 is necessary for production of 11-cis-vitamin A in the
638 retinal visual cycle. *Nat Genet* **20**, 344-351 (1998).
639 17. K. Takata, T. Kasahara, M. Kasahara, O. Ezaki, H. Hirano, Ultracytochemical localization
640 of the erythrocyte/HepG2-type glucose transporter (GLUT1) in cells of the blood-retinal
641 barrier in the rat. *Invest Ophthalmol Vis Sci* **33**, 377-383 (1992).
642 18. I. A. Simpson *et al.*, The facilitative glucose transporter GLUT3: 20 years of distinction.
643 *Am J Physiol Endocrinol Metab* **295**, E242-253 (2008).
644 19. S. Belhadj *et al.*, Long-Term, Serum-Free Cultivation of Organotypic Mouse Retina
645 Explants with Intact Retinal Pigment Epithelium. *J Vis Exp* 10.3791/61868 (2020).
646 20. X. Zhao *et al.*, Shikonin Inhibits Tumor Growth in Mice by Suppressing Pyruvate Kinase
647 M2-mediated Aerobic Glycolysis. *Scientific Reports* **8**, 14517 (2018).

648 21. A. Ortin-Martinez *et al.*, Number and distribution of mouse retinal cone photoreceptors:
649 differences between an albino (Swiss) and a pigmented (C57/BL6) strain. *PloS one* **9**,
650 e102392 (2014).
651 22. C. J. Jeon, E. Strettoi, R. H. Masland, The major cell populations of the mouse retina. *J*
652 *Neurosci* **18**, 8936-8946 (1998).
653 23. B. S. Winkler, Glycolytic and oxidative metabolism in relation to retinal function. *J Gen*
654 *Physiol* **77**, 667-692 (1981).
655 24. N. G. Abdulaev *et al.*, Nucleoside diphosphate kinase from bovine retina: purification,
656 subcellular localization, molecular cloning, and three-dimensional structure.
657 *Biochemistry* **37**, 13958-13967 (1998).
658 25. E. M. Rueda *et al.*, The cellular and compartmental profile of mouse retinal glycolysis,
659 tricarboxylic acid cycle, oxidative phosphorylation, and ~P transferring kinases.
660 *Molecular vision* **22**, 847-885 (2016).
661 26. P. Bai, Biology of Poly(ADP-Ribose) Polymerases: The Factotums of Cell Maintenance.
662 *Mol Cell* **58**, 947-958 (2015).
663 27. F. Paquet-Durand *et al.*, Excessive activation of poly(ADP-ribose) polymerase contributes
664 to inherited photoreceptor degeneration in the retinal degeneration 1 mouse. *J*
665 *Neurosci* **27**, 10311-10319 (2007).
666 28. R. E. Riepe, M. D. Norenburg, Müller cell localisation of glutamine synthetase in rat
667 retina. *Nature* **268**, 654-655 (1977).
668 29. R. A. Nathwani, S. Pais, T. B. Reynolds, N. Kaplowitz, Serum alanine aminotransferase in
669 skeletal muscle diseases. *Hepatology* **41**, 380-382 (2005).
670 30. W. R. Kim, S. L. Flamm, A. M. Di Bisceglie, H. C. Bodenheimer, Serum activity of alanine
671 aminotransferase (ALT) as an indicator of health and disease. *Hepatology* **47**, 1363-1370
672 (2008).
673 31. L. F. Barros, I. Ruminot, P. Y. Sandoval, A. San Martín, Enlightening brain energy
674 metabolism. *Neurobiol Dis* **184**, 106211 (2023).
675 32. W. Haq, E. Zrenner, M. Ueffing, F. Paquet-Durand, Using Micro-Electrode-Array
676 Recordings and Retinal Disease Models to Elucidate Visual Functions: Simultaneous
677 Recording of Local Electroretinograms and Ganglion Cell Action Potentials Reveals the
678 Origin of Retinal Oscillatory Potentials. *Bioengineering (Basel)* **10** (2023).
679 33. L. Wang, M. Kondo, A. Bill, Glucose metabolism in cat outer retina. Effects of light and
680 hyperoxia. *Invest Ophthalmol Vis Sci* **38**, 48-55 (1997).
681 34. D. Y. Yu, S. J. Cringle, E. N. Su, Intraretinal oxygen distribution in the monkey retina and
682 the response to systemic hyperoxia. *Invest Ophthalmol Vis Sci* **46**, 4728-4733 (2005).
683 35. A. Tolone *et al.*, The PKG Inhibitor CN238 Affords Functional Protection of
684 Photoreceptors and Ganglion Cells against Retinal Degeneration. *Int J Mol Sci* **24** (2023).
685 36. A. Söderpalm, A. Szél, A. R. Caffé, T. van Veen, Selective development of one cone
686 photoreceptor type in retinal organ culture. *Invest Ophthalmol Vis Sci* **35**, 3910-3921
687 (1994).
688 37. R. V. S. Rajala, Aerobic Glycolysis in the Retina: Functional Roles of Pyruvate Kinase
689 Isoforms. *Frontiers in Cell and Developmental Biology* **8** (2020).
690 38. M. M. Giarmarco *et al.*, Daily mitochondrial dynamics in cone photoreceptors. *Proc Natl*
691 *Acad Sci U S A* **117**, 28816-28827 (2020).
692 39. H. G. Joost, A. D. Habberfield, I. A. Simpson, A. Laurenza, K. B. Seamon, Activation of
693 adenylate cyclase and inhibition of glucose transport in rat adipocytes by forskolin

694 analogues: structural determinants for distinct sites of action. *Mol Pharmacol* **33**, 449-
695 453 (1988).
696 40. F. O'Leary, M. Campbell, The blood-retina barrier in health and disease. *Febs j*
697 10.1111/febs.16330 (2021).
698 41. R. Diaz-Ruiz, M. Rigoulet, A. Devin, The Warburg and Crabtree effects: On the origin of
699 cancer cell energy metabolism and of yeast glucose repression. *Biochimica et Biophysica*
700 *Acta (BBA) - Bioenergetics* **1807**, 568-576 (2011).
701 42. H. G. Crabtree, Observations on the carbohydrate metabolism of tumours. *Biochem J* **23**,
702 536-545 (1929).
703 43. R. J. Kessler, C. A. Tyson, D. E. Green, Mechanism of uncoupling in mitochondria:
704 uncouplers as ionophores for cycling cations and protons. *Proc Natl Acad Sci U S A* **73**,
705 3141-3145 (1976).
706 44. G. U. Balcke *et al.*, Linking energy metabolism to dysfunctions in mitochondrial
707 respiration--a metabolomics in vitro approach. *Toxicol Lett* **203**, 200-209 (2011).
708 45. L. L. Dugan *et al.*, Mitochondrial production of reactive oxygen species in cortical
709 neurons following exposure to N-methyl-D-aspartate. *J Neurosci* **15**, 6377-6388 (1995).
710 46. V. Schreiber, F. Dantzer, J. C. Ame, G. de Murcia, Poly(ADP-ribose): novel functions for
711 an old molecule. *Nat Rev Mol Cell Biol* **7**, 517-528 (2006).
712 47. A. Venkatesh *et al.*, Activated mTORC1 promotes long-term cone survival in retinitis
713 pigmentosa mice. *J Clin Invest* **125**, 1446-1458 (2015).
714 48. N. Aït-Ali *et al.*, Rod-derived cone viability factor promotes cone survival by stimulating
715 aerobic glycolysis. *Cell* **161**, 817-832 (2015).
716 49. D. Trifunović *et al.*, cGMP-dependent cone photoreceptor degeneration in the cpfl1
717 mouse retina. *J Comp Neurol* **518**, 3604-3617 (2010).
718 50. A. J. Mears *et al.*, Nrl is required for rod photoreceptor development. *Nat Genet* **29**, 447-
719 452 (2001).
720 51. M. Yang *et al.*, Expression of glucose transporter-2 in murine retina: Evidence for
721 glucose transport from horizontal cells to photoreceptor synapses. *J Neurochem* **160**,
722 283-296 (2022).
723 52. L. L. Daniele *et al.*, Glucose uptake by GLUT1 in photoreceptors is essential for outer
724 segment renewal and rod photoreceptor survival. *Faseb j* **36**, e22428 (2022).
725 53. C. F. Burant, G. I. Bell, Mammalian facilitative glucose transporters: evidence for similar
726 substrate recognition sites in functionally monomeric proteins. *Biochemistry* **31**, 10414-
727 10420 (1992).
728 54. H. Koepsell, Glucose transporters in brain in health and disease. *Pflugers Arch* **472**,
729 1299-1343 (2020).
730 55. V. Actis Dato, M. C. Sánchez, G. A. Chiabrando, LRP1 mediates the IGF-1-induced GLUT1
731 expression on the cell surface and glucose uptake in Müller glial cells. *Sci Rep* **11**, 4742
732 (2021).
733 56. S. S. Goldman, Evidence that the gluconeogenic pathway is confined to an enriched
734 Müller cell fraction derived from the amphibian retina. *Exp Eye Res* **50**, 213-218 (1990).
735 57. S. Black *et al.*, CODEX multiplexed tissue imaging with DNA-conjugated antibodies. *Nat*
736 *Protoc* **16**, 3802-3835 (2021).
737 58. K. F. LaNoue *et al.*, Role of specific aminotransferases in de novo glutamate synthesis
738 and redox shuttling in the retina. *J Neurosci Res* **66**, 914-922 (2001).

739 59. S. Veeravalli *et al.*, Flavin-Containing Monooxygenase 1 Catalyzes the Production of
740 Taurine from Hypotaurine. *Drug Metab Dispos* **48**, 378-385 (2020).
741 60. H. Ripps, W. Shen, Review: taurine: a "very essential" amino acid. *Molecular vision* **18**,
742 2673-2686 (2012).
743 61. H. Pasantes-Morales, L. D. Ochoa de la Paz, J. Sepúlveda, O. Quesada, Amino acids as
744 osmolytes in the retina. *Neurochem Res* **24**, 1339-1346 (1999).
745 62. K. Sumizu, Oxidation of hypotaurine in rat liver. *Biochim Biophys Acta* **63**, 210-212
746 (1962).
747 63. J. Zheng, Energy metabolism of cancer: Glycolysis versus oxidative phosphorylation
748 (Review). *Oncol Lett* **4**, 1151-1157 (2012).
749 64. T. Pfeiffer, S. Schuster, S. Bonhoeffer, Cooperation and competition in the evolution of
750 ATP-producing pathways. *Science* **292**, 504-507 (2001).
751 65. J. C. Lai, K. L. Behar, Glycolysis-citric acid cycle interrelation: a new approach and some
752 insights in cellular and subcellular compartmentation. *Dev Neurosci* **15**, 181-193 (1993).
753 66. J. Du *et al.*, Phototransduction Influences Metabolic Flux and Nucleotide Metabolism in
754 Mouse Retina. *J Biol Chem* **291**, 4698-4710 (2016).
755 67. R. Gebhard, Cytochemical demonstration of aspartate aminotransferase activity in the
756 rat retina. *Brain Res* **539**, 337-341 (1991).
757 68. J. R. Moffett, B. Ross, P. Arun, C. N. Madhavarao, A. M. A. Namboodiri, N-
758 Acetylaspartate in the CNS: from neurodiagnostics to neurobiology. *Progress in*
759 *neurobiology* **81**, 89-131 (2007).
760 69. S. Dadsetan *et al.*, Brain alanine formation as an ammonia-scavenging pathway during
761 hyperammonemia: effects of glutamine synthetase inhibition in rats and astrocyte-
762 neuron co-cultures. *J Cereb Blood Flow Metab* **33**, 1235-1241 (2013).
763 70. H. Igarashi, Y. Suzuki, V. J. Huber, M. Ida, T. Nakada, N-acetylaspartate decrease in acute
764 stage of ischemic stroke: a perspective from experimental and clinical studies. *Magn*
765 *Reson Med Sci* **14**, 13-24 (2015).
766 71. H. D. Yan, K. Ishihara, T. Serikawa, M. Sasa, Activation by N-acetyl-L-aspartate of acutely
767 dissociated hippocampal neurons in rats via metabotropic glutamate receptors.
768 *Epilepsia* **44**, 1153-1159 (2003).
769 72. J. Moffett, P. Arun, P. Ariyannur, A. Namboodiri, N-Acetylaspartate reductions in brain
770 injury: impact on post-injury neuroenergetics, lipid synthesis, and protein acetylation.
771 *Frontiers in Neuroenergetics* **5** (2013).
772 73. S. Alba-Arbalat *et al.*, In Vivo Molecular Changes in the Retina of Patients With Multiple
773 Sclerosis. *Investigative ophthalmology & visual science* **62**, 11-11 (2021).

774

775 **Figures and Tables**

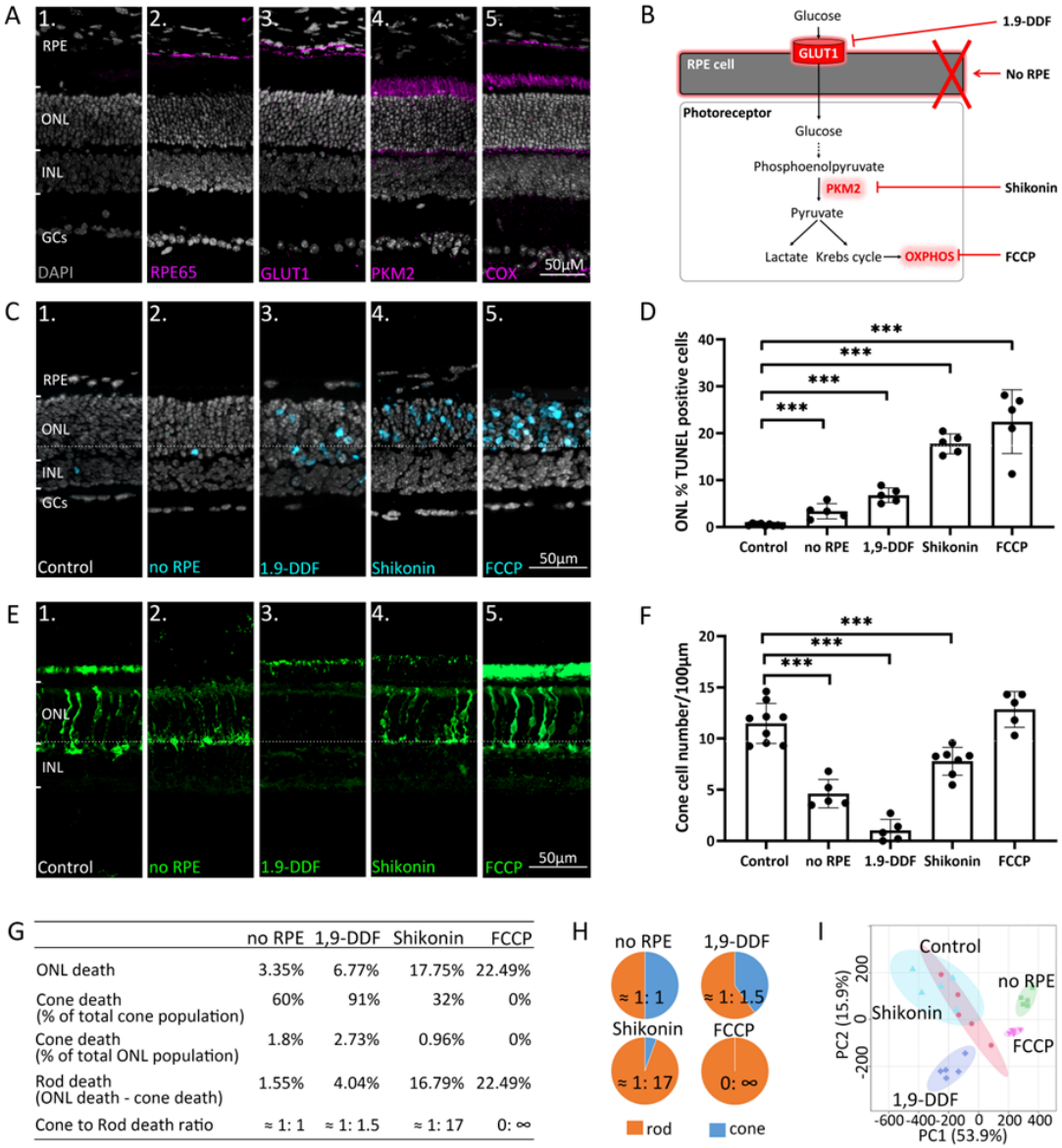

	no RPE	1,9-DDF	Shikonin	FCCP
ONL death	3.35%	6.77%	17.75%	22.49%
Cone death (% of total cone population)	60%	91%	32%	0%
Cone death (% of total ONL population)	1.8%	2.73%	0.96%	0%
Rod death (ONL death - cone death)	1.55%	4.04%	16.79%	22.49%
Cone to Rod death ratio	≈ 1: 1	≈ 1: 1.5	≈ 1: 17	0: ∞

776
777 **Figure 1. Manipulating energy metabolism differentially affects rod and cone photoreceptors.** (A)
778 Immunofluorescence staining of *in vivo* retina (magenta): (A1) negative control, (A2) RPE65, (A3) glucose
779 transporter-1 (GLUT1), (A4) pyruvate kinase M2 (PKM2), (A5) mitochondrial cytochrome oxidase (COX).
780 (B) Overview of experimental manipulations. Organotypic retinal explants were cultured for 6 days *in vitro*
781 with or without RPE or treated with 1,9-DDF, Shikonin, or FCCP. (C) TUNEL assay performed on *in vitro*
782 retina (cyan) marking dying cells in the five experimental conditions. (D) Quantification of TUNEL-positive
783 cells in outer nuclear layer (ONL). Data represented as mean ± SD. (E) Cone-arrestin labelling (green) in
784 the ONL. (F) Quantification of arrestin-positive cones. Data represented as mean ± SD. (G) Table giving
785 percentages of cones and rods lost for each treatment. (H) Pie charts illustrate cone to rod cell death
786 ratios. (I) Principal component analysis (PCA) of retinal samples investigated with ^{1}H-NMR spectroscopy-
787 based metabolomics. Dots in graphs represent individual retinal explants. Statistical testing: One-way
788 ANOVA with Tukey's post-hoc test. Asterisks indicate significance levels; *p*-values: *** < 0.001, ** < 0.01 *
789 < 0.05. RPE = retinal pigment epithelium; INL = inner nuclear layer; GCs = ganglion cells.
790

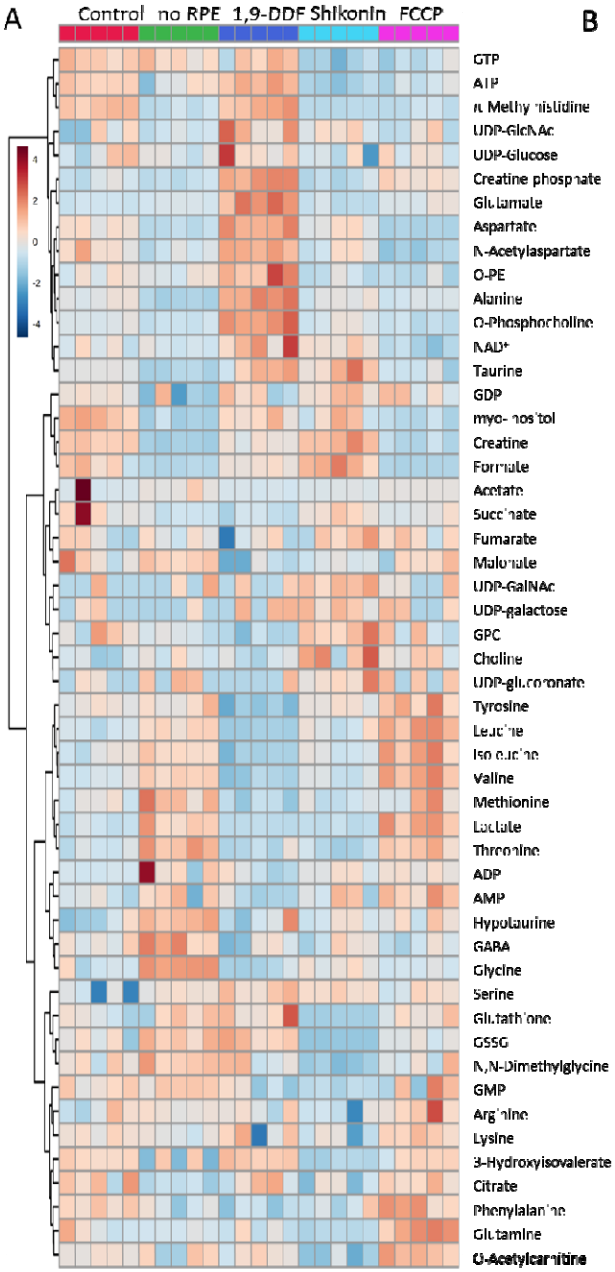

Class	Function	Metabolite	no RPE		1,9-DDF		Shikonin		FCCP	
			p	FC	p	FC	p	FC	p	FC
Nucleotides	Energy metabolism, cofactors	**ATP**	↓*	0.8	↑**	1.1	↓****	0.6	↓***	0.7
		ADP					↑*	1.3	↑***	1.5
		AMP							↑**	1.8
		GTP					↓****	0.6	↓***	0.7
		GDP								
		GMP					↓**	0.4		
	Coenzyme	**NAD+**			↑*	1.3			↓*	0.8
		UDP-GalNAc					↑*	3.2		
		UDP-GlcNAc			↑*	1.5				
Organic Acids	Glycolysis	Lactate	↑***	1.7					↑***	4.6
	Krebs cycle	Citrate	↓*	0.7						
		Fumarate								
		Succinate								
	Mitochondria	Formate	↓**	0.2					↓**	0.2
	Osmolyte	Taurine	↓****	0.9	↑*	1.1	↑*	1.1		
		Hypotaurine	↑***	1.9						
		GABA	↑**	1.1						
	Neuronal tissue-associated metabolite	Malonate			↓*	0.4				
		NAA	↓*	0.8	↑*	1.2			↓***	0.6
		Creatine	↓****	0.6	↓***	0.9			↓****	0.6
		Creatine phosphate			↑****	1.6			↑**	
Amino Acids	Neurotransmitter, Krebs cycle	Glutamate	↑**	1.1	↑****	2.1			↑**	1.2
	BCAA	Isoleucine	↑**	1.3	↓**	0.7			↑**	1.6
		Leucine	↑***	1.3	↓***	0.8			↑***	1.5
		Valine	↑****	1.3	↓**	0.8			↑***	1.5
	Glucogenic, ketogenic amino acid	Glutamine					↓*	0.7	↑*	1.5
		Tyrosine			↓****	0.7			↑*	1.7
		Lysine							↑*	1.1
		Phenylalanine	↓*	0.9	↓**	0.8	↓*	0.9		
		Aspartate	↓****	0.6	↑**	1.6			↓***	0.4
		Alanine	↓****	0.8	↑****	1.5			↓**	0.9
	Serine synthesis pathway, one carbon metabolism	Methionine	↑**	2.1	↓*	0.4				
		Serine	↑*	1.7	↑*	2.0	↑*	1.8		
		Glycine	↑****	1.6						
		Threonine	↑****	1.4					↑***	1.3
		π-Methyl-histidine	↓****	0.2			↓****	0.1	↓***	0.2
		N,N-Dimethyl-glycine	↑*	1.2			↓**	0.6		
Lipids and growth	β oxidation of fatty acids	O-Acetyl-carnitine					↓**	0.5	↑**	1.4
		3-Hydroxy-isovalerate			↑*	1.1	↓****	0.5		
	Cell membrane synthesis, Kennedy pathway	myo-Inositol	↓****	0.6					↓***	0.6
		Choline					↑*	1.7	↑*	1.3
		O-Phospho-choline	↓**	0.8	↑****	2.0			↓**	0.8
		GPC			↓*	0.8				
		O-PE			↑**	1.3	↓*	0.9	↓*	0.9
Tri-peptide	Redox metabolism	Glutathione					↓**	0.1		
		GSSG	↑*	1.8	↑*	1.8	↓**	0.1		

Figure 2. ^{1}H-NMR spectroscopy-based metabolomic analysis of retina subjected to interventions in energy metabolism. (A) Heatmap based on unsupervised hierarchical cluster analysis by Ward's linkage, showing auto-scaled metabolite concentrations (red – high, blue – low) in five different experimental conditions: control - red, *no* RPE - green, 1,9-DDF - dark blue, Shikonin - light blue, FCCP purple (n = 5 samples per condition). (B) Metabolic profiles of each intervention were compared to control. Metabolites significantly changed in at least one experimental condition were grouped according to functions and pathways. Data show *p*-values and fold change (FC) over control. Statistical comparison: Student´s unpaired *t*-test (group variance equal); *p*-values: **** < 0.0001, *** < 0.001, ** < 0.01 * < 0.05. See also Supplementary Figure 3.

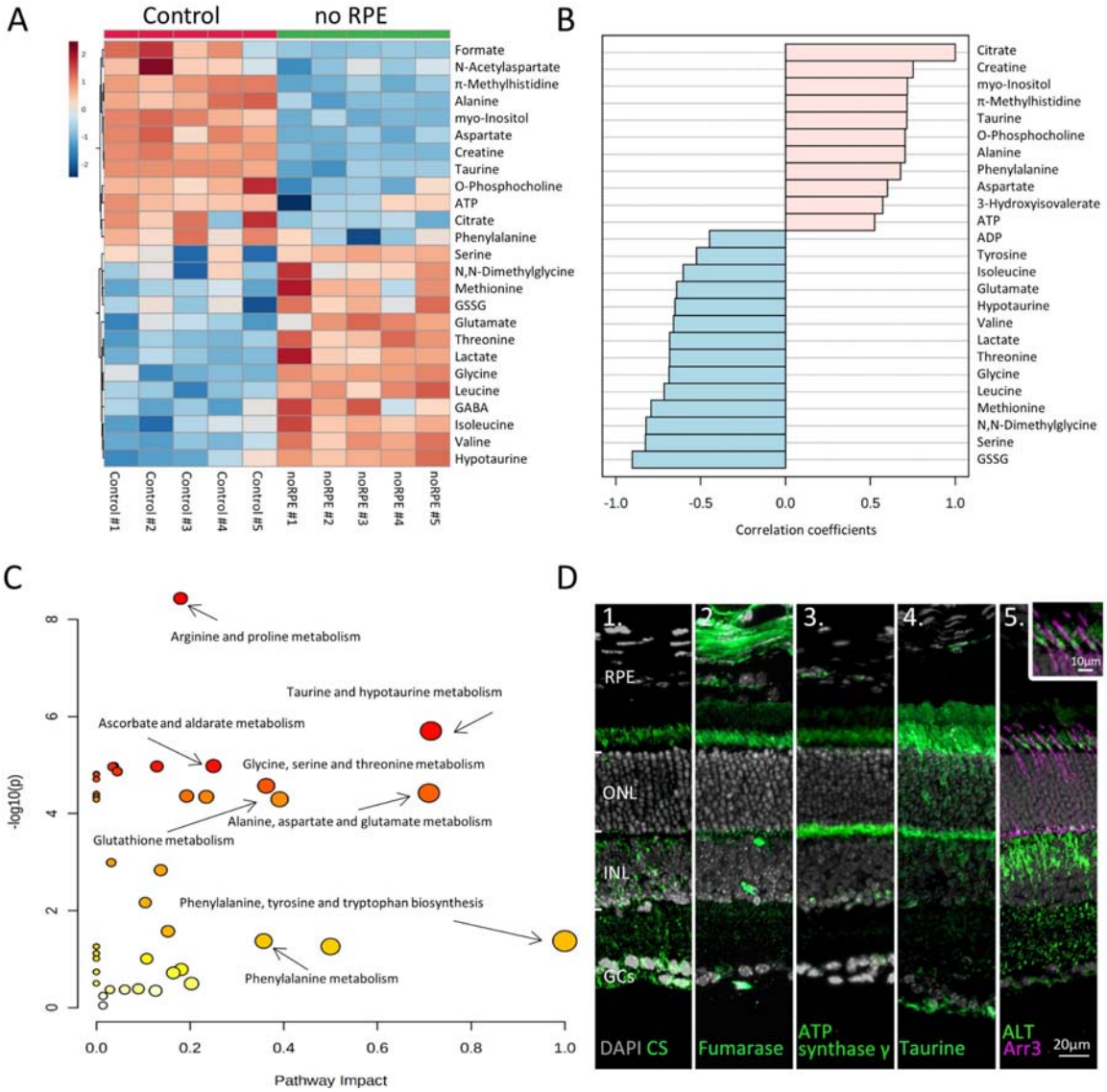

Figure 3. Absence of RPE dramatically changes retinal metabolism. (A) Heatmap, based on unsupervised hierarchical cluster analysis by Ward's linkage, illustrating statistically significant changes for 25 metabolites (unpaired *t*-test, fold change (FC) > 1.2, raw p value < 0.05). (B) Pattern hunter for citrate, showing the top 25 correlating metabolites, correlation coefficient given as Pearson r distance. (C) Metabolic pathways most affected in *no* RPE condition compared to control, based on KEGG- pathway database. (D) Immunodetection of enzymes and metabolites (green) on *in vivo* retina. (D1) citrate synthase (CS), (D2) fumarase, (D3), ATP synthase γ, (D4) taurine, (D5) alanine transaminase (ALT). Co-staining for ALT and cone arrestin (Arr3; magenta) showed high expression in cone inner segments. DAPI (grey) was used as a nuclear counterstain. See also Supplementary Figure 5.

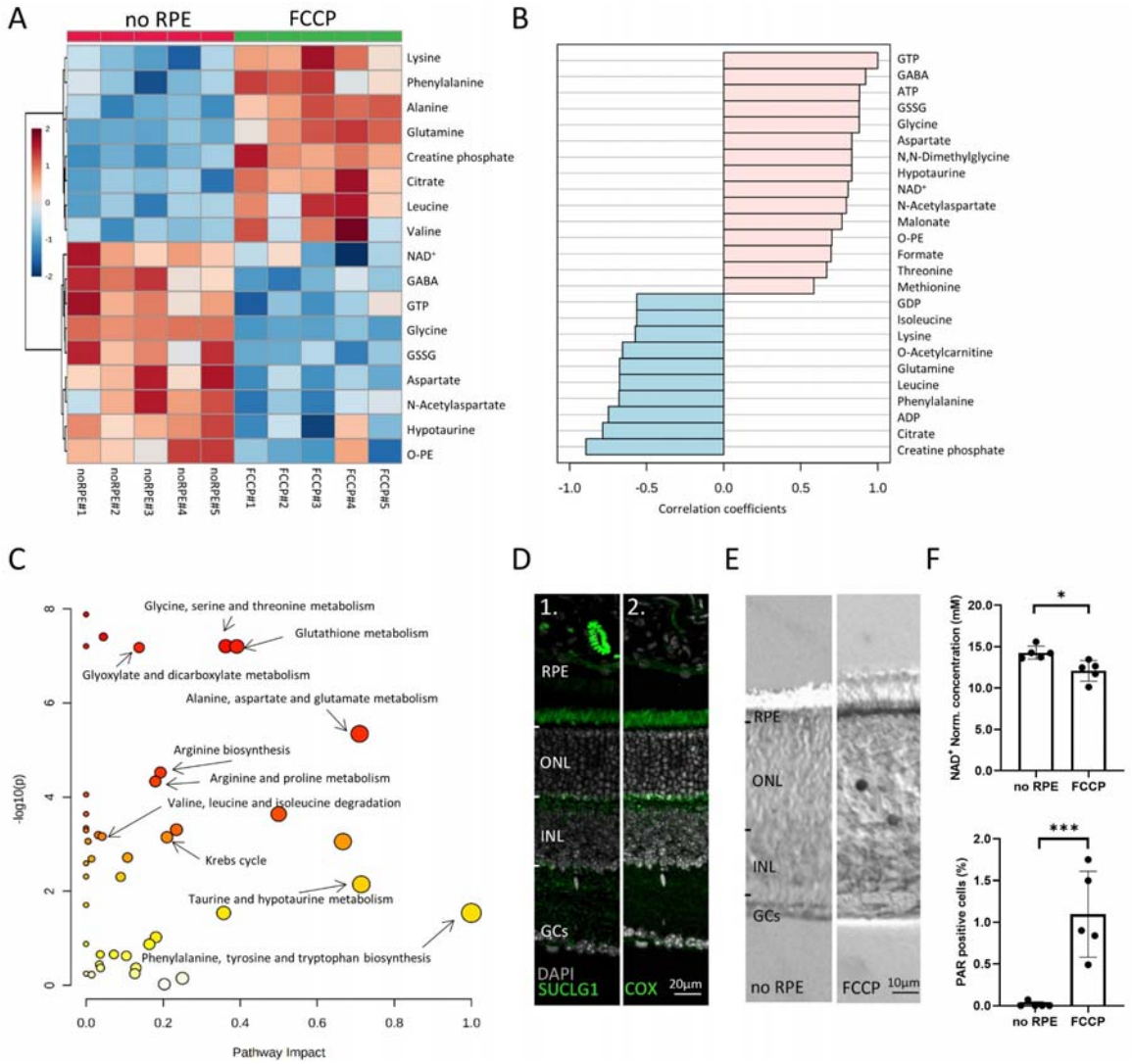

Figure 4. Comparison between *no* RPE and FCCP conditions. (A) Heatmap, based on unsupervised hierarchical cluster analysis by Ward's linkage, illustrating statistically significant metabolite changes (unpaired *t*-test, fold change > 1.2, raw *p*-value < 0.05). (B) Pattern hunter for guanosine triphosphate (GTP) showing the top 25 correlating compounds. Correlation coefficient given as Pearson r distance. (C) KEGG-based pathway analysis, comparison between *no* RPE and FCCP. (D) Immunofluorescence for succinate-CoA ligase-1 (SUCLG1, green) labelled photoreceptor inner segments and colocalized with COX. DAPI (grey) was used as a nuclear counterstain. (E) PAR positive photoreceptors (black) in the outer nuclear layer (ONL) of FCCP treated retina. (F) Compared to *no* RPE, NAD^+ levels were lower in the FCCP group, while the percentage of PAR positive cells was higher. Data represented as mean ± SD. Statistical testing: Student´s two-tailed *t*-test. *p*-values: *** < 0.001, * < 0.05. See also Supplementary Figure 7.

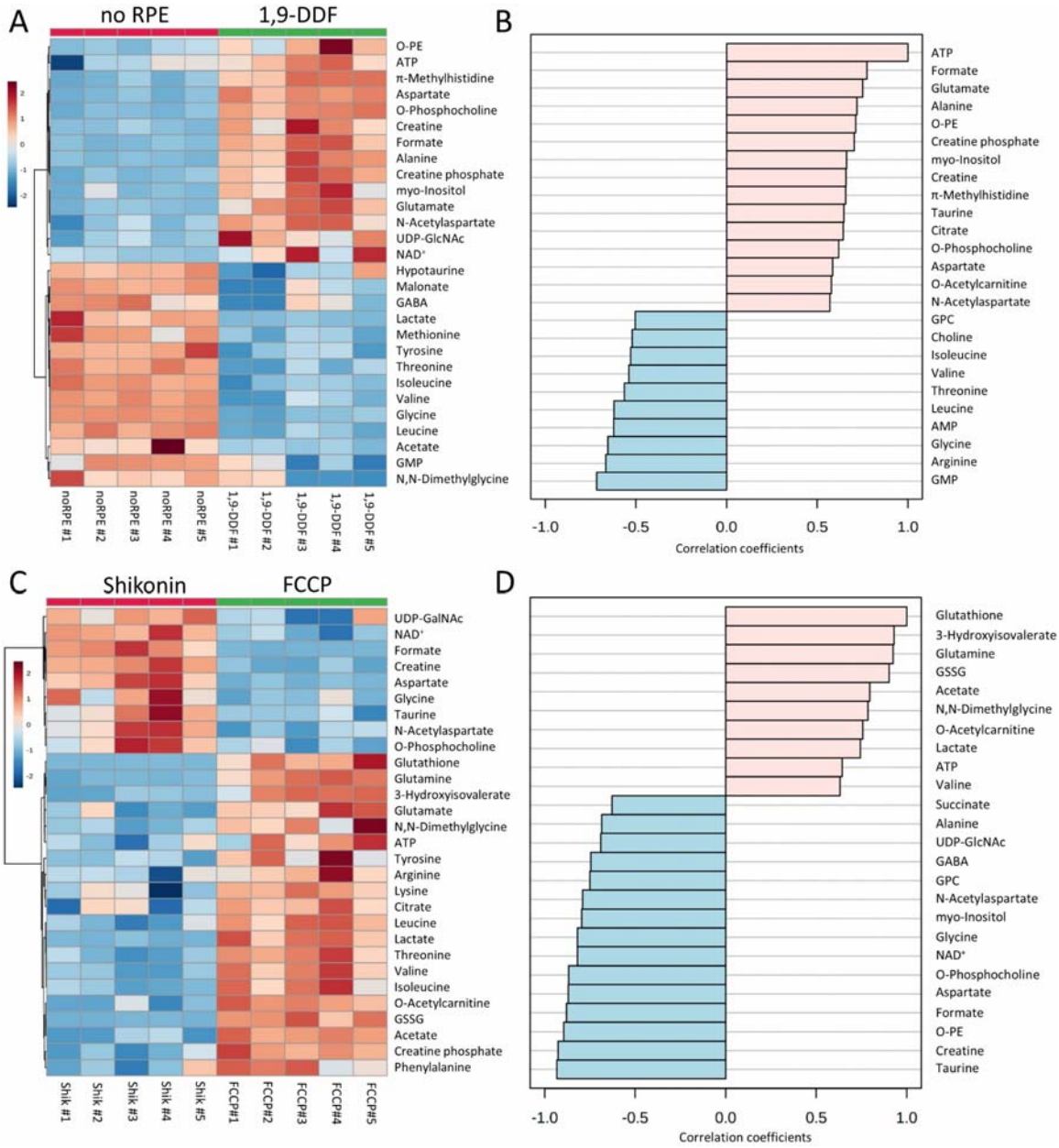

Figure 5. Metabolomic analysis of *no* RPE vs. 1,9-DDF treatment and Shikonin vs. FCCP treatment. Heatmap illustrating statistically significant metabolite changes (unpaired *t*-test, fold change (FC) > 1.2, raw p value < 0.05) for (A) *no* RPE vs. 1,9-DDF and (C) Shikonin vs. FCCP. Pattern hunter for (B) ATP and (D) glutathione, showing the top 25 correlating compounds. Correlation coefficient given as Pearson r distance. See also Supplementary Figures 8 and 9.

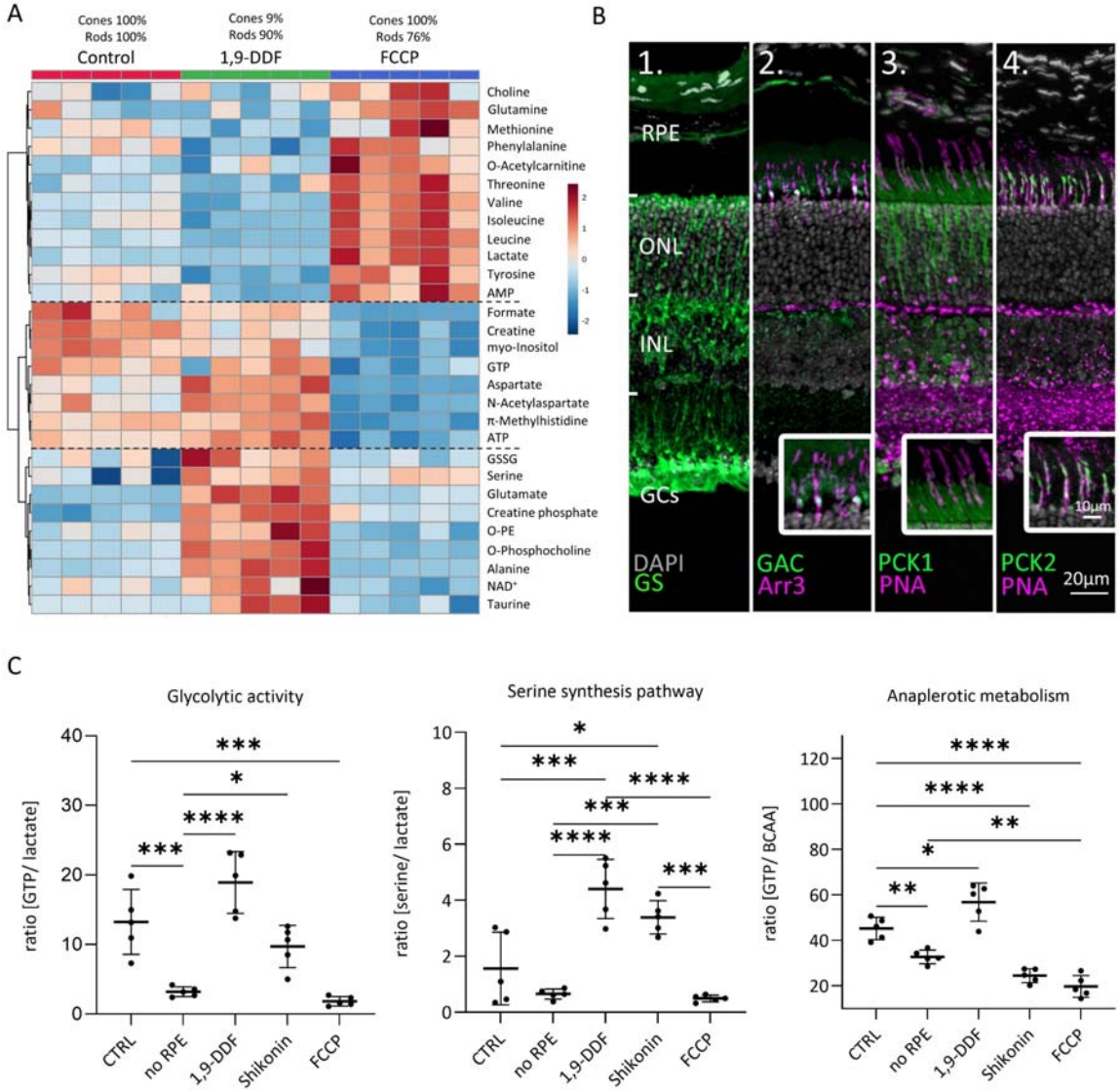

Figure 6. Metabolomic comparison between control, 1,9-DDF, and FCCP treatment. (A) Heatmap illustrating 29 statistically significant metabolite changes (parametric one-way ANOVA, Fisher's LSD post-hoc analysis). Three main clusters of metabolite changes were evident (dashed lines). (B) Immunostaining (green) for enzymes related to glutamine metabolism. DAPI (grey) was used as nuclear counterstain. (B1) Glutamine synthase (GS), (B2) glutaminase C (GAC); co-localization with cone-arrestin (Arr3; magenta). (B3) phosphoenolpyruvate carboxykinase 1 (PCK1) did not co-localize with cone marker peanut-agglutinin (PNA) while (B4) PCK2 did. (C) Ratios between metabolites representing glycolysis (lactate vs. GTP), anaplerotic metabolism (GTP vs. BCAA), and serine synthesis pathway (serine vs. lactate). Data represented as individual data points with mean ± SD. Statistical testing: One-way ANOVA with Tukey's post-hoc test; *p*-values: **** < 0.0001, *** < 0.001, ** < 0.01 * < 0.05. See also Supplementary Figure 10.

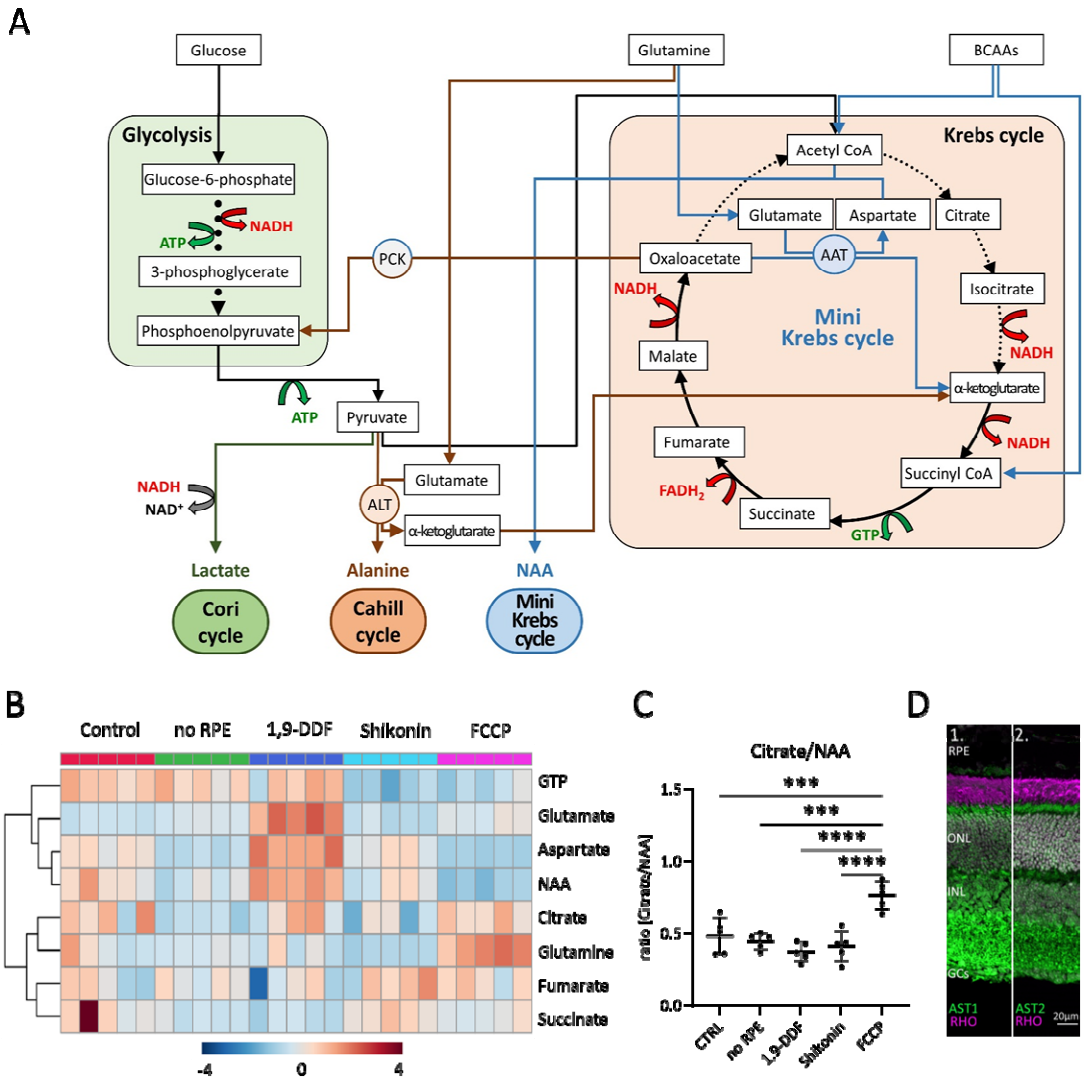

Figure 7. Metabolic pathways in the retina, key metabolites, and expression of aspartate amino transferase (AST). (A) Overview of main metabolic pathways and metabolites. Execution of Cori- (green arrows), Cahill- (brown), or mini-Krebs-cycle (blue) releases the signature metabolites lactate, alanine, and N-acetylaspartate (NAA), respectively. Key enzymes of the Cahill- and mini-Krebs-cycle are phosphoenolpyruvate carboxykinase (PCK), pyruvate kinase M (PKM), alanine transaminase (ALT) and AST. (B) Hierarchical clustering of eight metabolites connected to Krebs and mini-Krebs cycle. (C) Ratio NAA *vs.* citrate, representing full and mini-Krebs-cycle. Data represented as ratio of individual data points with mean ± SD. Statistical comparison using one-way ANOVA, Tukey's multiple comparisons test; *p*-values: **** < 0.0001, *** < 0.001. (D) Immunostaining for aspartate amino transferase-1 and -2 (AST1, AST2; green) co-stained with the rod photoreceptor outer segment marker rhodopsin (RHO; magenta), DAPI (grey) was used as nuclear counterstain.

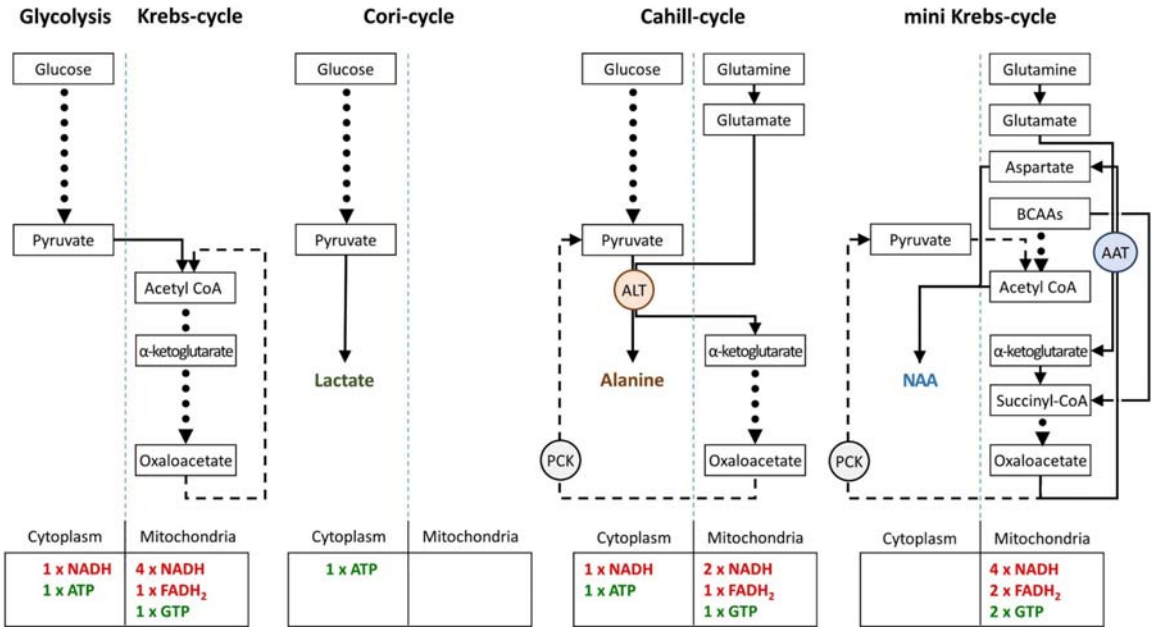

Figure 8. Comparison of metabolic pathways and their energetic efficiencies. Compared to the Cori-cycle, both Cahill- and mini-Krebs-cycles are highly efficient. Their key enzymes – alanine transaminase (ALT) and aspartate amino transferase (AST), respectively – generate alanine and aspartate/N-acetylaspartate (NAA). Pyruvate carboxy kinase (PCK), either in cytoplasm or within mitochondria, may reconstitute pyruvate from oxalacetate. Note that energy output of each pathway was calculated based on input of pyruvate (three carbons) or glutamate/branched-chain-amin-acid/acetyl-CoA (three carbons).